Direct Estimate of Lateral Eddy Diffusivity Upstream of the Drake Passage

ROSS TULLOCH, RAFFAELE FERRARI*, OLIVER JAHN

Massachusetts Institute of Technology, Cambridge, MA

ANDREAS KLOCKER

Australian National University, Canberra, Australia

JOSEPH LACASCE

Department of Geosciences, University of Oslo, Oslo, Norway

JIM LEDWELL

Woods Hole Oceanographic Institution, Woods Hole, Massachusetts

JOHN MARSHALL

Massachusetts Institute of Technology, Cambridge, MA

MARIE-JOSE MESSIAS

School of Environmental Sciences, University of East Anglia, Norwich, UK

KEVIN SPEER

Department of Earth, Ocean and Atmospheric Science, Florida State University, Tallahassee, Florida

ANDREW WATSON

School of Environmental Sciences, University of East Anglia, Norwich, UK

Corresponding author address: Raffaele Ferrari, Department of Earth, Atmospheric and Planetary Sciences,

Abstract

The first direct estimates of the rate at which geostrophic turbulence mixes tracers across the Antarctic Circumpolar Current are presented. The estimate is computed from the spreading of a tracer deliberately released upstream of Drake Passage as part of the Diapycnal and Isopycnal Mixing Experiment in the Southern Ocean (DIMES). The meridional eddy diffusivity, a measure of the rate at which the area of the tracer grows along an isopycnal across the Antarctic Circumpolar Current over time, is 710 ± 260 m^{2}s^{-1} at 1500m depth. The estimate is based on an extrapolation of the anthropogenic-tracer based diffusivity with estimates computed from numerical tracers in a 1/20th of a degree model simulation of the circulation and turbulence in the Drake Passage region. The model is shown to reproduce the observed spreading rate of the DIMES tracer and suggests that the meridional eddy diffusivity is weak in the upper kilometer of the water column straddling around 300 m^{2}s^{-1} and peaks at the steering level, where the eddy phase speed is equal to the mean flow speed, at 2 km. These vertical variations are not captured by ocean models used for climate studies, but they significantly affect the ventilation of different water masses.

Massachusetts Institute of Technology, 77 Massachusetts Avenue, Cambridge MA 02139.

E-mail: rferrari@mit.edu

1. Introduction

At the latitudes of the Antarctic Circumpolar Current (ACC), waters from the Atlantic, Indian and Pacific Oceans are brought to the surface by the Roaring Forties to be transformed into Subantarctic Mode Waters to the north and Antarctic Bottom Waters to the south (Marshall and Speer 2012). This global transformation of water masses is achieved by intense air-sea exchange of heat, fresh water, carbon, and other chemical tracers in the Southern Ocean and exerts a strong control on Earth's climate. Above the sill depth of the Drake Passage, the circulation is dominated zonally by the ACC and meridionally by the sum of a wind-driven meridonal overturning circulation (MOC) and an MOC driven by the turbulent eddies generated through instabilities of the ACC (Johnson and Bryden 1989; Speer et al. 2000; Marshall and Radko 2003). The air-sea fluxes and Earth's climate are therefore very sensitive to oceanic turbulence in the Southern Ocean. The current debate as to whether Southern Ocean carbon uptake will increase or decrease in a warming climate stems from different assumptions on the changes in oceanic turbulence (Russell et al. 2006; Abernathey et al. 2011).

Despite its importance for climate studies, there have not been direct observational estimates of the rate of mixing which drives the eddy-induced circulation across the ACC. Indirect estimates have been made, for example, by Stammer (1998) who used scaling laws and the surface geostrophic velocity from altimetry, and by Marshall et al. (2006) who drove numerical tracers by the altimetric velocity field. Phillips and Rintoul (2000) attempted to estimate the fluxes of heat and momentum from mooring data, but not the rate at which tracers are mixed. Here we present the first direct measurements based on the spreading of a tracer deliberately released as part of the Diapycnal and Isopycnal Mixing Experiment in the Southern Ocean (DIMES). The mixing is quantified in terms of an eddy diffusivity which is defined as the spreading time rate of the tracer, once it asymptotes a constant. The eddy diffusivity is a tensor $\mathbf{K}$ which quantifies the growth of the patch in all three dimensions. Here we will focus on the component of the diffusivity representing the tracer spreading along neutral density surface (isopycnal mixing) and across the ACC, because this is the component that drives the eddy-induced MOC and plays an important role in setting the strength of both the upper and lower overturning cells in the Southern Ocean. Ledwell et al. (2011)

reported on the diffusivity across neutral density surfaces (diapycnal mixing), which is believed to play an important role in the dynamics of the abyssal ocean. Our focus is on waters above the depths experiencing significant diapycnal mixing.

The goal of this paper is to infer an isopycnal diffusivity based on the lateral dispersion of the anthropogenic tracer released in DIMES. The tracer was released at 1500 m, at the interface between the upper and lower MOC cells, in the Pacific sector of the Southern Ocean 2300 km upstream of the Drake Passage. Ledwell et al. (2011) estimated that after one year the tracer spread to a Gaussian profile in density with a standard deviation of less than 30 m across the density that it was injected at. We can therefore assume that, at leading order, the tracer spread only along the target density surface.

Our analysis focuses on the first year of spreading when most of the tracer remained west of the Drake Passage; the center of mass of the tracer reached the Drake Passage after approximately two years. We focus on measurements collected in the sector upstream of the Drake Passage, because the ACC jets are mainly zonal there. Past Drake Passage, the jets strongly meander and it is difficult to separate along and across-jet dispersion. Furthermore the tracer sampling downstream of the Drake Passage is not adequate to determine the isopycnal diffusivity, but can be used to estimate the diapycnal diffusivity.

Due to the temporal and spatial scales involved, measuring isopycnal diffusivity by sampling a tracer spreading through the ocean is difficult, since only a fraction of the tracer distribution can be directly sampled. Some method must be developed to extrapolate the tracer measurements and infer where the unsampled tracer may have spread. Ledwell et al. (1998) estimated the isopycnal diffusivity in the North Atlantic assuming that the tracer spread diffusively as a Gaussian blob, which is a reasonable assumption in a region with weak mean flows. Fitting a Gaussian to the discrete tracer sampling, they were able to reconstruct the evolution of the whole tracer patch at all times. This approach cannot be used in the Southern Ocean, where the tracer is advected rapidly downstream by the meandering ACC jets, at the same time being dispersed meridionally by the turbulent eddies. Here, therefore, the tracer measurements have been extrapolated by simulating the DIMES tracer release with a numerical model of the region, run at $1/20^{th}$ of a degree horizontal

resolution. The model is compared against hydrography and mooring observations (see Appendix B)and provides a link between the sub-sampled tracer distributions and the full tracer distribution.

Using the tracer sampled during the one-year tracer survey (called "US2"), together with the numerical model, we estimate that the tracer experienced a meridional isopycnal diffusivity of 710 ± 260 m^{2}s^{-1} over the first year after release. This value agrees with an independent estimate based on the dispersion of approximately 50 acoustically-tracked isopycnal floats, deployed on the same isopycnal surface as the tracer (see LaCasce et al. 2013).

The isopycnal diffusivity estimated here is an isopycnal tracer diffusivity, not a lateral buoyancy diffusivity. That is we are discussing the Redi diffusivity, not the Gent-McWilliams diffusivity using the jargon of non-eddy resolving climate models (see the discussion in the textbook by Griffies 2004). The isopycnal diffusivity is also the diffusivity that mixes the active tracer potential vorticity thereby driving the overturning ocean circulation (e.g. Plumb 1986). The model suggests that the isopycnal tracer diffusivity increases from about 300 ± 250 m^{2}s^{-1} in the upper ocean to 900 ± 250 m^{2}s^{-1} at 2 km and decays rapidly below. The maximum in eddy diffusivity is near the steering level where the phase speed of the eddies equals the mean current speed. This is consistent with the suggestion that the zonal mean flows suppress mixing in the upper ocean, while the diffusivity is unsuppressed, and thereby enhanced, near the steering level between 1.5 km and 2 km (Smith and Marshall 2009; Abernathey et al. 2010; Klocker et al. 2012b). The values of the diffusivity at the steering level from here are on the low side of those reported in the literature which span 1000–3000 m^{2}s^{-1} (Smith and Marshall 2009; Klocker et al. 2012b; Abernathey et al. 2010). DIMES is the first study that relies on direct estimates of tracer spreading, while all previous studies were only indirectly constrained by data. Hence the DIMES estimates provide ground truth to derive better parameterizations of eddy mixing for climate models.

Our paper is organized as follows. The DIMES tracer release, sampling, measurements and uncertainty are discussed in Section 2. The numerical model and its comparison against observations are discussed in Section 3. Section 4 derives our best estimate of the eddy diffusivity based on DIMES data and model output. Section 5 describes the modeled estimates of the vertical dependence of diffusivity using a set of tracers released at different depths. Finally, we conclude in

Section 6.

2. The DIMES tracer release

In early February 2009 (Cruise US1), 76 kg of a passive chemical tracer (trifluoromethyl sulphur pentaflouride, CF_3SF_5) was released from the Research Vessel *Roger Revelle* on the 27.9 kg m^{-3} neutral density surface (near 1500 m depth) upstream of the Drake Passage (58°S, 107°W) between the SAF and the PF.

The tracer was released in a rough 'x' pattern in an area about 20 km across. The injection system was maintained within a few meters of the target isopycnal surface via a feedback control system, as described in (Ledwell et al. 1998). The tracer distribution was sampled within two weeks of the release, and found to be confined to within 20 meters of the target density surface (Ledwell et al. 2011). The tracer was intentionally released in fluid whose eastward motion was biased low, in order to facilitate initial sampling. The release location was guided by altimetry data indicating a stagnation point at depth, if the current had an "equivalent barotropic" structure (Killworth and Hughes 2002). Further evidence of a small velocity was obtained from a CTD survey conducted within 2 days of release in a 70-km box centered on the release. The magnitude of the geostrophic velocity at the center of the tracer patch estimated from this survey, with surface geostrophic velocity from altimetry as reference, was less than 0.03 m/s. Low velocity of the tracer patch was at least partially confirmed by the observation that all of the stations at which tracer was found during the initial survey, 4 to 14 days after release, were within 10 km of the center of the initial patch.

In kinematic simulations based on the altimetry at the time of the experiment (not shown), with velocity at the tracer depth approximated as 0.38 times the surface geostrophic velocity from the altimeter, the center of mass of the tracer moved slightly to the west at first, and did not start moving east until a month after release. Thus, the actual tracer movement might be expected to have been delayed by about a month relative to the mean of an ensemble of numerical releases in other representations of the flow field.

The spread of the tracer was sampled during Cruise US2 (see Table 1), a year after the release, using a conventional CTD/Rosette system. Water samples were analyzed using a method similar to that described in Ho et al. (2008). The uncertainty (1 standard deviation) of individual concentrations was no greater than 0.03 $\times 10^{-15}$ mol L^{-1}, or 5% of the concentration, whichever was greater. This uncertainty is small compared to the peak concentration measured during US2 of about 4×10^{-15} mol L^{-1}.

Fig. 1a shows the location of the initial tracer release on Cruise US1 (black dot) and the locations (circles) and normalized amounts of column-integrated tracer concentration measured (circle area) in the follow-up cruises: US2 (blue), UK2 (purple), UK2.5 (black) and US3 (red). The UK cruise tracks, which sample multiple transects, have been subdivided into individual transects UK2A, UK2B, UK2C, UK2.5A and UK2.5B. The areas of the circles in each cruise have been normalized by the maximum amount of tracer measured on that cruise, and the largest circles of each cruise have the same area (except US2 where due to high concentrations the largest circle has four times the area).

The column integral at each station was calculated by integrating over a profile obtained by interpolating linearly between the sample levels. Uncertainty of the column integrals is also less than 5%, which is very small compared with lateral variations, as assessed from the lateral autocorrelation of tracer integrals (not shown). The closest station spacing was 28 km, along the lines at 93°W and 96°W. The autocorrelation of column integrals of all station pairs with separation within 30 km (71 pairs) was only 0.4 ± 0.2. The autocorrelation decreases to 0 ± 0.2 for 121 pairs with separations between 90 and 120 km, which is less than the distance between major survey lines. Hence, accurate interpolation of the data to create a map is not possible even within the bounds of the survey. Furthermore, it is clear from the high levels of tracer found along the northern border of the survey (Fig. 1a) that although the survey may have delimited the tracer fairly well to the west and south, the patch was not delimited to the north and northeast.

The average of all the vertical profiles obtained during US2 was approximately Gaussian in shape with a standard deviation of 30 m, and with virtually all the tracer found within 100 m of the target density surface, as shown in Ledwell et al. (2011). Hence, one year after release, the vertical

spread of the tracer was of the same order as the vertical resolution of most ocean circulation models, including the one used in the present study. Incidentally, variations among profiles of the vertical distribution were small enough that the estimate by Ledwell et al. (2011) of the diapycnal diffusivity, and its uncertainty, in the region between the injection location and the US2 survey area were accurate, despite the variability of column integral within the patch and the failure of the survey to delimit the patch.

Figs. 1a and 2 show column-integrated tracer concentrations divided by the total amount of tracer released (circles, units m^{-2}) for each of the cruises. Only a subset of Cruise US2 is shown in Fig. 2, *i.e.*, the latitudinal transect at 96°W is denoted as 'US cruise 2A' and the latitudinal transect at 93°W is denoted as 'US cruise 2B'. The x's shown in Fig. 2 represent simulated concentrations, which will be discussed in Section 3b. The largest column integral measured during US2 were 3.46×10^{-9} mol m^{-2}, located at (94°W,56.66°S), which, after normalizing by the 387.6 mols of injected tracer, is 8.92×10^{-12} m^{-2}. The maximum relative concentrations during UK2, UK2.5 and US3 were 1.05×10^{-12} m^{-2}, 9.55×10^{-12} m^{-2}, and 6.30×10^{-12} m^{-2} respectively. The maximum during US2 is an outlier which is twice as large as the next largest value during US2, which is itself 50% larger than the next 5–10 datapoints. Notice that the scale of the vertical axis in Fig. 2 decreases in downstream cruises either because only the leading edge of the tracer patch is being sampled (UK2B, UK2C, UK25B) or the trailing edge of the tracer is being sampled (US3).

The distributions of the transects resemble three types of distributions: Gaussian, top-hat and multimodal. Gaussian distributions would result if the tracer spread by Fickian diffusion, top-hat distributions would result if the spread of the tracer encroached on meridional mixing barriers and multimodel distributions would result from a streaky tracer distribution, caused by filaments of tracer being carried by jets or eddies. Hints of Gaussian distributions are evident in UK2A, UK2B and UK25A, while UK2C and UK25B appear to have more of a top-hat distribution, and US2 and US3 appear to have multimodal distributions. Cruise US2 is the only cruise which samples the tracer in a close two dimensional grid, hence it is the only cruise which can measure the propagation of the tracer's center of mass. The blue 'x' in Fig. 1b shows the center of mass of the DIMES tracer during US2, computed as the simple sum $\overline{\mathbf{x}} = \sum_i (\mathbf{x}_i c_i) / \sum_i c_i$, implying a slight

southward displacement (about 0.75° latitude) and a mean zonal propagation speed of about 2.3 cm s^{-1} over the first year of dispersal.

3. The Drake Patch model

The simulated tracer data presented here is from a series of virtual tracer releases, which replicate the DIMES release, using a regional setup of the MITgcm (Marshall et al. 1997a,b), herein referred to as the "Drake Patch". The model's horizontal grid resolution is $1/20^{th}$ of a degree (a resolution of 3km$\times$6km at the location of the tracer injection), spanning across the Drake Passage from 160°W to 20°W in longitude and from 75°S to 35°S in latitude. The vertical mesh grid is divided into 100 layers of unequal thickness such that the top 70 layers, which span the top 1900 m, are all less than 35 m thick[1].

The European Centre for Medium-Range Weather Forecasts (ECMWF) Interim Reanalysis (ERA-Interim, Simmons et al. 2006) 6-hour winds and buoyancy fluxes force the model's surface, and the Ocean Comprehensive Atlas (OCCA, Forget 2009) provides monthly transports, heat and salt fluxes as well as sea ice area and thickness at the lateral boundaries. Initial model conditions are an interpolation of the $1^\circ \times 1^\circ$ resolution OCCA state on January 1, 2005, and the model cycles repeatedly over the years for which OCCA is defined (2004–2006). The simulations are intended to capture the statistics of the seasonal cycle of the Southern Ocean near the Drake Passage rather than predict the specific ocean state at the time of the DIMES tracer release. The model domain (excluding where restoring is applied to the OCCA state estimate) is shown in Figs. 3 and 4. A more detailed description of the model setup is given in Appendix B.

[1]Layer spacing $\Delta z \leq 35$ m allows the vertical grid to resolve Gaussian tracer profiles with a root mean square (rms) spread (σ_z) as small as 70 m (Hill et al. 2012) and most importantlyensures that spurious numerical diffusion in the vertical is below 10^{-5} $m^2 s^{-1}$, consistent with directestimates of diapycnal diffusivity from the DIMES tracer release Ledwell et al. (2011).

3a. *Comparison of the model with observations*

We begin by comparing the Drake Passage transports, eddy kinetic energy and temperature-salinity hydrography with the Drake Patch simulation. The vertically integrated zonal transport across the Drake Passage has a a mean of 152 Sv and standard deviation of 3 Sv in the Drake Patch simulation, consistent with the transport entering from the open western boundary from OCCA (152 Sv, Forget 2009). This transport is somewhat larger than past estimates (137$\pm$ 7 Sv, Meredith et al. 2011), but agrees with more recent ones (Firing et al. 2011, 154$\pm$ 38 Sv). We show below that tracers injected in the model move eastward at the same rate as the tracer released in DIMES further confirming that the model eastward transport is consistent with observations.

The initial and boundary conditions in the Drake Patch are derived from the $1^\circ \times 1^\circ$ OCCA climatology which does not resolve eddies. Upon spinning up, boundary currents, baroclinic and barotropic instabilities and topographic steering quickly develop, in $\mathcal{O}(50)$ days, at and downstream of the Drake Passage (east of 75°W), as well as far upstream at the Udintsev and Eltanin fracture zones (between 145°W and 135°W). After $\mathcal{O}(100)$ days, a vigorous mesoscale eddy field is established in these regions. Weaker mesoscale eddies develop locally near the US2 region after $\mathcal{O}(300)$ days, and a significant amount of eddy energy is advected into the US2 region from the fracture zones to the west. An earlier model configuration, which had its western boundary at 115°W and so lacked the upstream fracture zones and exhibited only about 60% of the eddy kinetic in a region near US2 (90°W – 100°W and 60°S–55°S) compared to the current configuration. Therefore, a significant amount of the eddy energy between 100°W and 80°W is advected into that region from the fracture zones at 140°W, despite the advective timescale for eddies to propagate 50 degrees downstream at 2.3 cm s^{-1} being about 4 years and the timescale of local baroclinic instability being less than a year (Tulloch et al. 2011). The simulation which includes Udintsev and Eltanin also exhibits relatively more inter-annual variability of kinetic energy than the simulation without them and takes about twice as long to roughly equilibrate at the surface (about 800 days versus 400 days to reach 90% of surface KE after 5 years).

Figs. 3 and 4 compare mean and eddy current speeds in the Drake Patch model with AVISO altimetric observations. The model and the observations agree rather well, although the model's

eddy kinetic energy is about 10% larger than AVISO near the US2 cruise track shown in Fig. 1a. The model's time-mean flow $(\overline{u}, \overline{v})$ is computed from a 3 year time-mean, while the AVISO speeds are based on a 19 year time-mean (1993-2011), so more eddy aliasing is present in the model time-means than in the AVISO time-means. This aliasing is likely responsible for some of the small scale features in the in the model average.

The model has a southward flowing boundary current off the coast of Chile that ejects northwest propagating anticyclonic eddies into the Pacific Ocean which is absent in the observations. These eddies are generated by the large freshwater fluxes along the Chilean coast[2] and they propagate away from the DIMES region, thus they are not expected to influence the tracer distribution in the model during the first two years.

Fig. 5 compares the vertical structure of simulated root-mean-square current speed against observations from the First Dynamic Response and Kinematic Experiment (FDRAKE) moorings located in the Drake Passage during the late seventies (Pillsbury et al. 1979; Nowlin, Jr. et al. 1982). The moorings were deployed for an average of about 320 days and are compared to a 3 year average in the model. The model and observations are in good agreement, although the model is somewhat more energetic than the observations. One likely reason for the excess energy is that while mesoscale eddies are resolved, bottom boundary layer turbulence (Scott et al. 2011) and lee wave generation (Nikurashin and Ferrari 2011; Nikurashin et al. 2013), are not, so the modeled eddies experience too little bottom dissipation. The very energetic model vertical profile that lies to the left of all other profiles in Fig. 5 comes form the location of the northernmost mooring, which is close to the model's strong boundary current, visible in Fig. 3b. The discrepancy is probably not very significant, because this current exhibits significant year to year variability in the model. Regardless, our analysis focuses on mixing away from these boundary current.

Temperature, salinity and neutral density in the model upstream of the Drake Passage agree well with CTD data from the World Ocean Circulation Experiment (WOCE). In Appendix B,

[2] An experiment with the atmospheric forcing shifted 20° west resulted in the generation of anticyclones 20 degrees west of the Chilean coast. These anticyclones appear to be driven by freshwater forcing at the surface, as that region is one of the rainiest in the world, *e.g.*, Villa Puerto Edén receives almost 6 m of rain per year. They are likely sensitive to the ERA reanalysis product and its low resolution, which does not limit the heavy rain to the coastline.

Sections P18, P19C/S and A21 from WOCE are compared with the model solution. The model receives large scale hydrographic information from OCCA at the western and northern boundaries, so the upstream sections in the model largely resemble OCCA and therefore observations. Within Drake Passage, the Polar Front appears to be shifted north by about one degree and is somewhat more intense. Section A21 appears to slice through a recirculation just north of 58°S in both observations and the model, a feature that is amplified in the model. The multi-yearn sea ice extent, shown in Fig. 1a, is in reasonable agreement with observations.

3b. *Comparison with DIMES tracer measurements*

We repeated 12 tracer injection experiments using the Drake Patch model. In each experiment the tracer was injected at the location of US1 in the DIMES field experiment. They were released 10 days apart from January through March of the 6$^{\text{th}}$ year of model integration. The initial tracer distribution was a Gaussian blob in x, y and z ($\sigma_x = \sigma_y = 20$ km, $\sigma_z = 75$ m), with the vertical distribution centered on the 59$^{\text{th}}$ model layer (1512 m depth), which is closest to the ρ_n =27.9 kg m^{-3} neutral density surface in the model in February.

Fig. 1a shows a snapshot of column integrated tracer concentration (in units of m^{-2}) after 365 days of integration for the ensemble member released on February 4 of the 6$^{\text{th}}$ year of model integration. The tracer concentration shown is normalized by the maximum concentration in the domain and all values between 0.5 and 1 have a uniform red tone. The distribution of the modeled tracer is directly comparable to the tracer concentrations measured during the US2 cruise, one year after the DIMES release and shown as blue circles. tracer concentrations from later cruises (UK2A, UK2.5, US3) are also shown for reference. Concentrations are shown as circles of different colors for each cruise. The circle diameters are proportional to the tracer concentration normalized by the largest tracer concentration found in that cruise, i.e. the circle diameter is a measure of how much tracer was found at that location compared to the largest value in that cruise.

The model tracer is still streaked into numerous filaments after one year (Fig. 1a. Much of the streakiness is eliminated in Fig. 1b which shows the distribution of the ensemble average of all 12 tracers, 365 days after each of their respective starting times have been equated. The blue ‘x’ in

Fig. 1b marks the center of mass of tracer collected during cruise US2 of the DIMES experiment, while the black 'x' ('+') marks the center of mass of the model ensemble average tracer sampled along the US2 cruise track (over the whole domain) at $t = 365$ days. The excess zonal distance travelled by the modeled ensemble (1.2°) corresponds to an excess zonal propagation speed of about 0.22cm s^{-1} over the first year, compared to the DIMES propagation speed of 2.3 cm s^{-1}. This difference is consistent with the fact that the DIMES tracer was purposefully released at a stagnation point in the altimetric velocity field, so that it did not move east until a month after release, as discussed in Section 2.

Fig. 2 shows transect-by-transect comparisons of tracer concentrations observed in DIMES (gray circles) and the simulated ensemble average (black x's) for each of the cruises. Note that US2 has been split into its two main transects at 96°W (denoted US2A) and 93°W (US2B). The comparison indicates that, at least until UK25, the propagation and dispersion of the observed and simulated tracers are consistent. The ensemble tracer is generally less streaky than the observations because it is an average over 12 tracers. Some differences can be seen for the US3 transect. The model has more tracer north of 59°S than the observations and the observed tracer distribution is multimodal, while the modeled concentration appears to be more Gaussian.

The time evolution of the mean and standard deviations of the modeled tracer concentration on the US2 cruise track stations are shown as black lines in Fig. 6a and 6c. The red x's mark the observed values, normalized by the total amount of tracer released. The mean concentration along a cruise track is defined as $\mu = N^{-1} \sum_i c_i$ and the standard deviation is defined as $s_N = \sqrt{(N-1)^{-1} \sum_i (c_i - \mu)^2}$, where N is the number of cruise track stations. The concentrations c_i (in mol L^{-1}) have been column-integrated and normalized by the number of mols of CF_3SF_5 injected. The mean concentration reaches a maximum in the first 200 days and then decays, while the standard deviation, a measure of the streakiness peaks at about 50 days. At the time of US2, the modeled streakiness has decayed to about $1/8^{\text{th}}$ of its initial peak, as a result of lateral homogenization of the streaks. Both the modeled mean and standard deviations agree with observations, *i.e.,* the red error bar, defined as a 95% confidence interval using bootstrapping of the observed concentrations, overlaps the gray shading, which is the range spun by the modeled

ensemble members.

A summary comparison of the modeled and observed mean and standard deviations of tracer concentration along each of the cruise tracks, at the times of each cruise, is in Fig. 6b and 6d. Consistent with Fig. 2, the mean and variance of concentrations on all of the cruises are consistent with observations, although the modeled concentrations are slightly larger for the US3 transect. The excess concentration in the model at the northwest-most station of US3 indicate that the DIMES tracer might have taken a slightly more southerly path than the modeled tracer. UK25A and UK25B in Fig. 2 seem to be in agreement with this hypothesis, however UK2A and UK2B do not. Fig. 14f in Appendix B shows that the Polar Front in the model is displaced northwards compared to observations and probably explains these discrepancies..

4. Using passive tracers to estimate dispersion and isopycnal eddy diffusivity

In this section, we outline how we estimate the eddy diffusivity from the dispersion of a passive tracer released from a point source. We focus on cross-current diffusivity because it is the component that supports the MOC. Consider the advection and diffusion of a passive tracer c by an incompressible flow field $\mathbf{u}$,

$$\partial_t c + \mathbf{u} \cdot \nabla c = \kappa \nabla^2 c, \tag{1}$$

where κ is the molecular diffusivity. Taking the average over an ensemble of such tracers, $\overline{c}$, yields

$$\partial_t \overline{c} + \overline{\mathbf{u}} \cdot \nabla \overline{c} = -\nabla \cdot \overline{\mathbf{u} c'} + \kappa \nabla^2 \overline{c}, \tag{2}$$

where c' are departures from the ensemble mean tracer. Further assuming small molecular diffusivity and a diffusive downgradient relationship between the eddy tracer flux and the mean tracer gradient gives

$$\partial_t \overline{c} + \overline{\mathbf{u}} \cdot \nabla \overline{c} = \nabla \cdot (\mathbf{K} \cdot \nabla \overline{c}), \tag{3}$$

where $\mathbf{K}$ is the eddy diffusivity tensor. Ledwell et al. (2011) showed that the diapycnal component of the diffusivity tensor upstream of the Drake Passage is of the order of 10^{-5} m^{2}s^{-1}. This implies

that the tracer only dispersed to an rms spread of about 30 m after one year, i.e. the tracer stayed close to its target density surface. The Drake Patch model also has low diapycnal diffusivity $K^z < 10^{-5}$ m^{2}s^{-1} (see Appendix B) and therefore we will consider $\overline{c}$ to be a column integrated tracer which is advected two-dimensionally along the target neutral surface.

Given a two-dimensional flow field, one can define a streamline coordinate system and derive expressions for the cross-stream tracer moments and eddy diffusivity (see Appendix A). In the simple case of uniform zonal streamlines ($\overline{u}(x,y,z) = u_0$) with the tracer center of mass at $y = 0$, the growth of the second meridional moment of a tracer following Eq. (3) is,

$$\partial_t < y^2\overline{c} >= 2 < (\partial_x K^{yx} + \partial_y K^{yy})y\overline{c} + K^{yy}\overline{c} >, \tag{4}$$

where $< \cdot >$ denotes area integration over x and y, and K^{yy} and K^{yx} are elements of $\mathbf{K}$. When the eddy statistics are independent of x and y, $\mathbf{K}$ is a constant and the components K^{xy}, K^{yx} and K^{xx} drop out of the across-stream moment equations (this is shown in Appendix A for a general stream coordinate system), so the cross-stream eddy diffusivity reduces to

$$K^{yy} = \frac{1}{2}\partial_t \sigma_y^2, \text{ where } \sigma_y^2 = \frac{< y^2\overline{c} >}{< \overline{c} >}. \tag{5}$$

Hence one can estimate K^{yy} from the asymptotic growth of the second y-moment of the tracer concentration, after initial transients have settled.

For a meandering mean flow, one ought to use a coordinate system that tracks the mean streamlines in order to separate the the eddy mixing along and across the mean flow. In Appendix A, we show how to extend the expression for the eddy diffusivity to a curvilinear coordinate system (s, ψ), where s is the along-stream coordinate and ψ is the cross-stream coordinate. While the cross-streamlines eddy diffusivity is mathematically well defined, it depends on curvature terms that are difficult to calculate accurately. Here, we chose to restrict the analysis upstream of the Drake Passage, west of 75°W, where the flow is mainly zonal and free of the strong meanders that exist downstream. The analysis in Appendix A confirms that the meridional and cross-streamline estimates of the eddy diffusivity are indistinguishable within error bars in the upstream region. In the interest of simplicity, we hence focus on the estimates of meridional diffusivity K^{yy}.

Another important consideration is whether we can assume that the longitudinal and latitudinal variations of K^{yy} in the ACC sector are small. Figs. 3 and 4 suggest that both the mean and the eddy kinetic energies are uniform over the region of the tracer during the first year after injection (see Fig. 1.) It is therefore sensible to assume that the meridional diffusivity does not vary much spatially. This is confirmed by the analysis to follow, which shows that K^{yy} does asymptote to a constant value over the first year–K^{yy} would continue to vary, if the tracer kept sampling regions with different dispersion rates.

Last, but not least, it is worth pointing out that the diffusivity based on spreading of a tracer along isopycnals is an estimate of the Redi (1982) diffusivity and not of the Gent and McWilliams (1990) diffusivity. The Gent and McWilliams diffusivity relates the horizontal buoyancy flux to the horizontal buoyancy gradient. Buoyancy is not conserved along horizontal planes, because of the vertical advection of stratification. Vertical advection does not affect the spreading of tracers along isopycnals.

4a. *Estimates of dispersion from a deliberate tracer release*

First we estimate the dispersion of the DIMES tracer after one year (US2) using available observations. Since only a fraction of the tracer was sampled during US2, any attempt of inferring the dispersion will be stymied by substantial uncertainty. We attempt to quantify this uncertainty by comparing a number of different approaches to estimating the rate of spreading experienced by the tracer after one year.

We consider three approaches to estimating the spreading of the tracer given by the centered second y-moment σ_y^2. The first method is a direct estimate of the second moment $\sigma_y^2 = N^{-1}\sum_{i=1}^{N} y_i'^2 c_i$ where N is the number of stations occupied in US2, y_i' is the latitude of station i minus the latitude of the tracer center of mass, and c_i is the vertically integrated tracer concentration measured at that station. In the second method, the binned second moment, we first average all c_i in latitude bins, that is we average over longitude to obtain an estimate of the concentration as a function of latitude only. Then the centered second moment is computed from the concentration as a function of latitude. The third method does a least-squares Gaussian fit to the tracer concentration

binned as a function of latitude and σ_y^2 is estimated as the variance of the Gaussian. In Appendix B we show that similar results are found using streamline coordinates, i.e. the spreading across streamlines is equal to the meridional spreading in the Drake Patch.

Estimates of σ_y^2 using each method are shown in Fig. 13. Each method has its strengths and weaknesses. The second moment method equally weights each datapoint assuming they are independent, and therefore tends to underestimate the dispersion when there is more sampling in the middle of the tracer distribution and when a significant fraction of the tracer is meridionally outside of the US2 sampling grid. The binned second moments alleviate the oversampling bias by first averaging tracer concentrations longitudinally and results in a slightly larger estimate. The bins are of equal width so bins averages are given equal weights. Binning introduces a new discretization error, but we found that binned estimates converged if more than 10 bins are used. The final method takes the binned values and minimizes the fit to a Gaussian distribution, to infer missing tracer. Rough interpolation estimates suggest that just less than 50% of the DIMES tracer was observed during US2, so fitting a Gaussian to the US2 data results in larger dispersion estimates.

Apart from the uncertainty due to the incomplete sampling of the tracer, additional uncertainty arises from converting the estimates of tracer dispersion into an estimate of eddy diffusivity. The eddy diffusivity is the asymptotic growth rate of σ_y^2. If the dispersion proceeded at the same rate throughout the whole year, then

$$K^{yy} = \frac{1}{2}\frac{d\sigma_y^2}{dt} = \frac{\sigma_y^2(1\text{year}) - \sigma_y^2(0)}{2\text{years}} \approx \frac{\sigma_y^2(1\text{year})}{2\text{years}}. \tag{6}$$

However initial transients are expected during which the growth of the second moment is not linear in time. We return to this issue below, when we repeat the dispersion calculations with the numerical model. For the moment we treat Eq. (6) as an ansatz.

Table 2 reports estimates of K^{yy} based on Eq. (6) and the three methods outlined above for estimating $\sigma_y^2(1\text{year})$. Using the direct estimate of the second moment $K^{yy} = 407$ m^{2}s^{-1}, while for the binned second moment $K^{yy} = 524$ m^{2}s^{-1} and the least-squares fit to a Gaussian gives $K^{yy} = 708$ m^{2}s^{-1}. The second moment $K^{yy} = 407$ m^{2}s^{-1} is shown in Fig. 7 as a red 'x'. The errors bars around the 'x' in Fig. 7 correspond to the bracketed uncertainty ranges in Table 2, which are 95% confidence intervals computed by bootstrapping the sample data 10000 times.

Values of the eddy diffusivity K^{nn} in streamlines coordinates are also reported in Table 2. These are obtained applying Eq. (6), but using σ^2_ψ instead of σ^2_y. They are substantially more uncertain, because of the additional complication of defining what are the proper mean streamlines. They will not be discussed further, because analysis of the tracer spreading in the numerical model suggests that there is no advantage working in streamline coordinates in the region considered where the mean flow are very close to zonal.

The large range in estimates of eddy diffusivity confirms that incomplete sampling of the tracer contributes a large uncertainty. Furthermore, as will become more clear, all estimates ignore initial transients during which the growth of σ^2_y is likely not linear in time. The model tracer release experiments will now be analyzed to gain insights on how to quantify both effects and obtain more robust estimates of the eddy diffusivity.

4b. *Estimates of dispersion and diffusivity from numerical tracers*

The model is used to address three aspects of the tracer dispersion. First, we want to know whether the eddy diffusivity asymptotes to a constant over the first year. Second, we need to know whether we can use Eq. (6) to estimate the diffuisivity. Third, we will consider the effect of under-sampling the tracer on estimates of the eddy diffusivity.

The blue line in Fig. 8a shows $\sigma^2_y(t)$ computed as the second moment of the ensemble tracer, i.e. the average over the 12 numerical injection experiments, using only tracer upstream of 75°W. East of 75°W, the tracer first gets squeezed into the Drake Passage and then veers north with the ACC resulting is rapid changes in the eddy statistics. For the first 500 days, out of the 1000 shown in the figure, the second moment increases approximately linearly in time. This confirms that the second moment of the tracer reaches a diffusive spreading within one year and it is sensible to represent this process with a constant eddy diffusivity.

The spreading of the ensemble mean tracer, the blue line in Fig. 8a, is not diffusive from day one. There is small initial transient in the first 100 days when $\sigma^2_y(t)$ does not grow linearly with time. In order to assess whether this transient invalidates the use of Eq. (6), we least-squares fitted a line to $\sigma^2_y(t)$ between $t = 100$ days and $t = 500$ days (black line in Fig. 8a), and compared it to

the red line which simply connects $\sigma_y^2(0)$ to $\sigma_y^2(1\text{year})$. The slope of the two lines are similar, 800 and 900 m^2s^{-1} respectively, suggesting that the ansatz of Eq. (6) is accurate to within 10%. Notice, however, that these estimates are based on an ensemble averaged tracer. In the DIMES experiment we have only one realization. In Fig. 8b we show, for each tracer release experiment, the half slopes estimated from linear least-squares fits between $t = 100$ days and $t = 500$ days, black 'x', versus the half slopes obtained from Eq. (6), red 'x'. Due the initial transient, estimates of K^{yy} based on Eq. (6) in the individual realizations vary from 718–966 m^2s^{-1}, whereas the dispersion rate from 100 to 500 days varies 727–861 m^2s^{-1}, which is a tighter bound on the diffusivity. Nevertheless the differences between the two estimates are quite small and on average no larger than in the ensemble mean. We conclude that Eq. (6) can be used to estimate K^{yy} from data with perhaps a 20% uncertainty.

A larger issue in estimating the diffusivity is the extrapolation of the subsampled tracer on the US2 grid points to the full tracer distribution. Fig. 7 shows half the second moment of the US2 subsampled tracer divided by time (red line) and that for the full tracer upstream of the Drake Passage (black line); these are estimates of K^{yy} based on Eq. (6) applied at all times instead of only at one year. The red line is 60% smaller than the black line implying that the US2 grid samples barely more than half of the tracer distribution. The ratio of the two curves is fairly constant between 250 and 450 days suggesting that estimates of K^{yy} based on sampling the tracers along the US2 grid after one year are biased 60% low.

The analysis presented so far suggests that Eq. (6) is appropriate to estimate K^{yy}, if the tracer is sampled adequately. Fig. 12 confirms that the estimate of K^{yy} is independent of the specific method used to estimate σ_y^2, when the calculation is applied to all of the tracer upstream of 75°W. However incomplete tracer sampling, as in the case of the DIMES experiment, is a serious limitation. Fig. 13 and Table 3 report estimates of K^{yy} computed using only data on the US2 cruise track. We repeated the same analysis followed for the DIMES observations and used Eq. (6) with the three different approaches to estimate σ_y^2. The results are reported in Table 3. The model confirms that the second moment and the binned second moment methods strongly underestimate K^{yy}. The Gaussian fit method correctly extrapolates the missing tracer when applied to the ensemble

averaged tracer on the US2 grid, but returns widely varying results when applied to a single tracer injection experiment. The inescapable conclusion is that none of the three approaches can be used to infer the spreading rate experienced by the tracer in DIMES, because the uncertainty associated with the missing tracer is too large.

Alternatively one can use the model estimate of K^{yy}, since the model has been tested against data. However a comparison of data and model estimates based on tracer data on the US2 cruise track shows that the model estimates are biased high: see Tables 2 and 3 and Fig. 7. Although it is true that the error bars are large enough to make all estimates consistent (the model uncertainty is estimated as the range of values obtained from the 12 tracer release experiments, while the DIMES uncertainty is computed using bootstrapping.) However the high model bias is consistent with the model kinetic energy being somewhat too high as discussed in Section 3a. Our conclusion is that the best way forward is to extrapolate the K^{yy} estimate from the DIMES data on the US2 cruise track using the model to infer the bias introduced because of the subsampling of the tracer. This is done in the next section.

4c. *Best estimate of the eddy diffusivity upstream of the Drake Passage at 1500 m*

The tracer dispersion estimated from the DIMES data in Section 4a is likely an underestimate because only half of the tracer was sampled and large values to the north suggest more dispersion northward. Since the model consistently overestimates the tracer dispersion compared to the DIMES observations, it cannot be used directly to estimate the DIMES diffusivity. We showed that by fitting a Gaussian meridionally to the subsampled tracer a Gaussian returned a diffusivity of $K^{yy} \approxeq \sigma_y^2(1\text{year})/2\text{years} \approx 708$ m^{2}s^{-1}, but the uncertainty in this value is large (see Table 2). Alternatively, the model can be used to infer how much of the tracer dispersion was missed by sampling only on the US2 cruise track.

Fig. 7 shows an extrapolation of the observed σ_y^2 from the US2 cruise multiplied by the ratio of the modeled σ_y^2 on the US2 cruise track only (red line) and on the full domain west of 75°W (black

line),

$$\text{Extrap } \sigma_y^2 = \frac{\text{Full modeled } \sigma_y^2}{\text{Modeled } \sigma_y^2 \text{ on US2}} \cdot \text{Obs } \sigma_y^2. \tag{7}$$

The error in the extrapolated σ_y^2 is estimated as

$$\text{Extrap Err} = \text{Extrap } \sigma_y^2 \cdot \sqrt{\left(\frac{\text{Obs Err}}{\text{Obs } \sigma_y^2}\right)^2 + \left(\frac{\text{Mod Spread on US2}}{\text{Mod } \sigma_y^2 \text{ on US2}}\right)^2}. \tag{8}$$

The modeled spread is calculated as the 95% confidence interval of the ensemble tracer dispersion on US2 computed using bootstrapping and are shown as grey shading in Fig. 7. The model spread of the full modeled σ_y^2 has not been included in the error estimate to avoid double counting. The observational error is estimated using bootstrapping and is shown as a red bar in Fig. 7.

The red 'x' in Fig. 7 marks the eddy diffusivity estimated using data along the US2 stations, while the blue 'x' is the extrapolated value. The last two rows of Table 2 summarize the results. Using this extrapolation we estimate that the meridional eddy diffusivity in the DIMES experiment was 710 ± 260 m^{2}s^{-1} at 1500m. This value agrees well with the estimate using a least-squares Gaussian fit building confidence in our estimate.

5. Estimating the vertical structure of the eddy diffusivity

There is growing evidence that the isopycnal eddy diffusivity of passive tracers varies in the vertical and has subsurface maxima (Treguier 1999; Smith and Marshall 2009; Abernathey et al. 2010; Lu and Speer 2010; Klocker et al. 2012b), unlike the horizontal buoyancy diffusivity which appears to be less variable in the vertical. It is therefore difficult to interpret the significance of the DIMES estimate and compare it to previous work without some information about the vertical variations from the 710 m^{2}s^{-1} value. We use the Drake Patch model to extrapolate the DIMES observations to the rest of the water column.

In order to assess the vertical variations of eddy diffusivity in the DIMES region, we run an ensemble of tracers injected on February 4 of the 6$^{\text{th}}$ year of model integration at 11 different depth between 500m and 3500m. The time evolution of σ_y^2 over time, estimated as the second moment of the tracer west of 75°W, is shown as blue lines for four selected depths in Fig. 9. After an

initial transient of about 100 days, the shallowest tracer disperses approximately linearly with time until about $t = 500$ days. Afterwards the dispersion accelerates as most of the tracer has reached the Drake Passage (not shown). The red lines are the dispersion experienced by the tracer over the first year and its slope is given by Eq. (6); this is the estimate of the diffusivity used for the DIMES tracer in Section 4. The black line shows a linear least-squares fit to the dispersion between $t = 95$ days and $t = 495$ days, which attempts to remove the initial transient from the diffusivity estimate. For tracers released in the upper 1000m the slopes of the red and black curves are very different, because the effect of the initial transient is significant. It is actually difficult to select the time window over which the growth rate of σ_y^2 is linear and a diffusivity can be defined. The ACC flow gets stronger toward the surface and the tracer does not have much time to diffusive before it reaches the Drake Passage: once the center of mass of the tracer reaches the Drake Passage, the flow first converges, resulting in a meridional squeezing of the tracer cloud, and then it veers north.

Fig. 10a shows the vertical profile of the the diffusivity K^{yy} estimated by least-squares fitting lines between $t = 100$ days and $t = 500$ days (black line). The figure shows the range of eddy diffusivity estimates from all the 12 ensemble members released at 1500m to emphasize that much uncertainty remains when the eddy diffusivity is estimated from a single release experiment. For comparison we also report our best estimate of the eddy diffusivity from the DIMES tracer release. The model estimate is biased slightly too high, but well within the observational error bar.

Despite the uncertainty, Fig. 10a shows that the eddy diffusivity has a maximum between 1000m and 2500m. Naively one may expect the eddy diffusivity to scale with the eddy kinetic energy, which is monotonously decreasing with depth as shown in Fig. 10b. However Bretherton (1966) and Green (1970) pointed out that mixing is strongly suppressed when eddies propagate at a speed different from the mean flow. Fig. 10b shows both that mean flow speed as a function of depth, averaged over the patch extending from 10W to 80W and 61S to 56S, and the eddy propagation speed, estimated with a radon transform of the sea surface height in the same region (see Smith and Marshall 2009). The eddy propagation speed is much smaller than the mean flow speed in the upper kilometer resulting into a suppression of the eddy diffusivity. Close to the steering level, where the mean flow equals the eddy propagation speed, there is no suppression and the eddy

diffusivity is largest. Similar vertical profiles of eddy diffusivity have been reported in recent studies of ACC flows more or less constrained to observations (Smith and Marshall 2009; Abernathey et al. 2010; Lu and Speer 2010; Klocker et al. 2012b).

Based on the model results, we infer that the meridional eddy diffusivity in the DIMES region peaks at around 900 m^{2}s^{-1} between 1000m and 2500m, while it is smaller than 500 m^{2}s^{-1} in the upper kilometer. While this structure is consistent with recent studies, the absolute values of the diffusivity are less so. In particular Abernathey et al. (2010) and Klocker et al. (2012b) published larger estimates for the DIMES region. Abernathey et al. (2010) estimated the diffusivity advecting tracers with a state estimate of the Southern Ocean Circulation and reported values around 500 m^{2}s^{-1} in the upper kilometer and values in excess of 2000 m^{2}s^{-1} at the steering level. Klocker et al. (2012a) estimated, using an idealized two-dimensional zonally re-entrant setup driven by surface altimetry, that the eddy diffusivity in the DIMES region peaked at 1000 m^{2}s^{-1} at 1.5 km depth, decreasing to 700 m^{2}s^{-1} at the surface. Most likely these differences stem from the different velocity fields use in the calculation and, in the case of Abernathey et al. (2010), from the use of a different method to compute the eddy diffusivity–they used Nakamura's definition of the eddy diffusivity. We contend that our estimate is more robust than these previous ones, because it is grounded in direct observations.

6. Discussion

This paper presents the first direct estimate of the isopycnal eddy diffusivity across the ACC just upstream of Drake Passage. The estimate was computed from the spreading of the DIMES tracer which was released in February, 2009. Using tracer sampling at one year after release (cruise US2) we estimated an isopycnal eddy diffusivity of 710 ± 260 m^{2}s^{-1} upstream of Drake Passage at 1500m. The estimate is based on the tracer spreading measured during US2 supplemented by a numerical model used to infer where the full tracer patch had spread after one year; US2 sampled only half of the tracer that was injected one year earlier.

In a companion paper LaCasce et al. (2013) find similar values of isopycnal eddy diffusivity

from floats released during the DIMES field campaign and floats released in the same numerical model used in our study of tracer dispersion. This builds confidence that our estimate is robust.

The numerical model further suggests that the isopycnal eddy diffusivity at 1500 m depth is close to its maxim in the water column. Diffusivities in the upper kilometer and below 3500m appear to be smaller than 500 m^{2}s^{-1}. The maximum in eddy diffusivity coincides with the steering level where the eddy propagation speed of 1 cm s^{-1} matches the zonal mean flow (Fig. 10). This vertical profile is consistent with the notion that mixing is suppressed in the upper kilometer of the ocean where eddies propagate much slower than the strong ACC flow, while it is large at the steering level where there is no suppression (Bretherton 1966; Green 1970; Ferrari and Nikurashin 2010). The mixing suppression at the surface and enhancement at depth is a robust feature of ocean mixing that has already been reported in idealized studies of channel flows (Treguier 1999; Smith and Marshall 2009), studies informed by ACC observations (Abernathey et al. 2010; Lu and Speer 2010; Klocker et al. 2012b) and observations (Naveira Garabato et al. 2011).

The present results have important implications for ocean models.The diffusivity estimated here is the Redi isopycnal diffusivity which homogenizes tracers and potential vorticity (Griffies 2004). Our result is that the Redi diffusivity in a sector of the Southern Ocean varies in the vertical with a peak of approximately 700 m^2/s at 1500m. If these variations are not local to the region sampled in DIMES, they imply strongest ventilation at the interface between the upper and lower meridional overturning cells (Marshall and Speer 2012) a region crucial for ocean carbon uptake. The implications for the horizontal buoyancy (Gent-McWilliams) diffusivity are more subtle. Smith and Marshall (2009) and Abernathey et al. (2013) find that the buoyancy diffusivity is more vertically constant than the tracer diffusivity, and has a magnitude close to the surface value of the tracer diffusivity. If this holds true in general, our results imply that the buoyancy diffusivity is less than 500 m^2/s, a value smaller than presently used in ocean models used for climate studies. However we realize that our results apply only to a small sector of the Southern Ocean upstream of the Drake Passage and one cannot extrapolate the results to the global ocean. Rather our analysis provide a ground-truth for developing parameterizations, which can then be used to extrapolate our results to other regions. This is currently being done at MIT (Bates et al., 2013).

Acknowledgement We wish also to thank all the scientists and ship crews of DIMES for their many contributions to a very successful experiment. NSF support through award OCE-1233832 is gratefully acknowledged. Computing resources on Pleiades and Yellowstone proved essential to perform the numerical simulations that are used to interpret the data.

APPENDIX A

Computation of tracer dispersion

Isopycnal mixing by geostrophic eddies is generally strongly anisotropic, being much larger along mean currents than across. It is therefore necessary to rotate coordinates along and across mean streamlines to properly estimate mixing in the two directions. We could not find a description of how to compute eddy diffusivities in a streamline coordinate system and so we decided to include in this appendix the details involved in the calculations. The second section of the appendix then compares estimate the dispersion in streamline and longitude-latitude coordinates for the DIMES region.

a. *Tracer moments in streamline coordinates*

Consider a 2D streamline coordinate system (s,ψ) where s is the along-stream coordinate (with units of length) and ψ is the cross-stream coordinate which increases normal ($\hat{\mathbf{n}}$) to the stream, *i.e.,*

$$\hat{\mathbf{s}} = \frac{(-\psi_y, \psi_x)}{|\nabla\psi|}, \qquad \hat{\mathbf{n}} = \frac{\nabla\psi}{|\nabla\psi|}.$$

as shown in the Fig. 11 below.

The first step is to write in streamline coordinate the conservation equation for the ensemble average tracer $\overline{c}$ advected by a two-dimensional streamfunction ψ,

$$\partial_t \overline{c} + J(\psi, \overline{c}) = -\nabla \cdot \mathbf{F}, \tag{9}$$

where J is a two-dimensional Jacobian and $\mathbf{F}$ represents the eddy flux of tracer. The eddy flux is assumed to be down the mean tracer gradient

$$\mathbf{F} = -\mathbf{K} \cdot \nabla\overline{\mathbf{c}}, \tag{10}$$

where $\mathbf{K}$ is a diffusivity tensor which is decomposed into anti-symmetric and symmetric components as $\mathbf{K} = \mathbf{K^{asym}} + \mathbf{K^{sym}}$. The anti-symmetric and symmetric tensors can be written as

$$\mathbf{K^{asym}} = \begin{pmatrix} 0 & -K^a \\ K^a & 0 \end{pmatrix}, \qquad \mathbf{K^{sym}} = \begin{pmatrix} K^{ss} & K^{sn} \\ K^{ns} & K^{ss} \end{pmatrix}. \tag{11}$$

The flux term in streamlines coordinates takes the from,

$$\nabla \cdot \mathbf{F} = |\nabla\psi| \left[\frac{\partial}{\partial s} \left(\frac{\mathbf{F} \cdot \hat{\mathbf{s}}}{|\nabla\psi|} \right) + \frac{\partial}{\partial \psi} \left(\mathbf{F} \cdot \hat{\mathbf{n}} \right) \right] \tag{12}$$

Now we want to take the streamline integral of the tracer equation. Young (1981, pg. 84, Eq. 9.13) skecthes how to take the average of a generic function $F(x, y)$ along an arbitrary streamline, ψ as

$$I(\psi) = \int_{R_\psi} F(x, y) dA.$$

The integral along a streamlines is therefore given by,

$$\begin{aligned} \frac{dI(\psi)}{d\psi} &= \lim_{\Delta\psi \to 0} \frac{I(\psi + \Delta\psi) - I(\psi)}{\Delta\psi} \\ &= \lim_{\Delta\psi \to 0} \frac{1}{\Delta\psi} \left[\int_{R_\psi + \Delta\psi} F(x, y) ds \frac{d\psi}{|\nabla\psi|} - \int_{R_\psi} F(x, y) ds \frac{d\psi}{|\nabla\psi|} \right] \\ &= \oint_{\partial R_\psi} F \frac{ds}{|\nabla\psi|}. \end{aligned}$$

Integrating the tracer equation along streamlines gives

$$\partial_t \oint_{\partial R_\psi} \overline{c} \frac{ds}{|\nabla\psi|} + \oint_{\partial R_\psi} \nabla\overline{c} \cdot d\mathbf{s} = \oint_{\partial R_\psi} \left[\frac{\partial}{\partial s} \left(\frac{\mathbf{K}\nabla\overline{\mathbf{c}} \cdot \hat{\mathbf{s}}}{|\nabla\psi|} \right) + \frac{\partial}{\partial \psi} \left(\mathbf{K}\nabla\overline{\mathbf{c}} \cdot \hat{\mathbf{n}} \right). \right] ds$$

Assuming that the streamline average extends all the way to where the tracer concentration vanishes, one has,

$$\partial_t \oint_{\partial R_\psi} \overline{c} \frac{ds}{|\nabla\psi|} = \oint_{\partial R_\psi} \frac{\partial}{\partial \psi} \left(\mathbf{K}\nabla\overline{\mathbf{c}} \cdot \hat{\mathbf{n}} \right) ds.$$

Expanding $\mathbf{K}$ into its tensor components gives

$$\partial_t \oint \overline{c} \frac{ds}{|\nabla\psi|} = \oint \frac{\partial}{\partial \psi} \left((K^a + K^{ns}) \frac{\partial \overline{c}}{\partial s} + K^{nn} |\nabla\psi| \frac{\partial \overline{c}}{\partial \psi} \right) ds. \tag{13}$$

Under the assumption that the diffusivity tensor is independent of the along stream coordinate, *i.e.*, $\mathbf{K} = \mathbf{K}(\psi)$, the $\partial_s \overline{c}$ term in Eq. (13) integrates to zero so the cross-stream diffusivity K^{nn} is the only component that evolves the stream-averaged tracer.

Further integrating Eq. (13) over the cross-stream coordinate gives the equation for the tracer averaged over the full domain, $< \psi \overline{c} >$,

$$\partial_t < \overline{c} >= \partial_t \iint \overline{c} \frac{ds}{|\nabla \psi|} d\psi = \iint \frac{\partial}{\partial \psi} \left(K^{nn} \nabla \overline{c} \cdot \hat{\mathbf{n}} \right) d\psi ds = 0.$$

Integrating the first moment with respect to ψ gives,

$$\begin{aligned} \partial_t < \psi \overline{c} > &= \iint \psi \frac{\partial}{\partial \psi} \left(K^{nn} \nabla \overline{c} \cdot \hat{\mathbf{n}} \right) d\psi ds \\ &= \iint \left(\frac{\partial K^{nn}}{\partial \psi} |\nabla \psi|^2 + \frac{1}{2} K^{nn} \frac{\partial}{\partial \psi} |\nabla \psi|^2 \right) \overline{c} \; dA, \end{aligned} \tag{14}$$

which implies a shift of the center of mass towards larger ψ, if either the diffusivity or the mean flow increase with ψ ($\partial_\psi K^{nn} > 0$ or the streamlines become more packed).

Integrating the second moment with respect to ψ gives

$$\begin{aligned} \partial_t < \psi^2 \overline{c} > &= \iint \psi^2 \frac{\partial}{\partial \psi} \left(K^{nn} \nabla \overline{c} \cdot \hat{\mathbf{n}} \right) d\psi ds \\ &= 2 \iint \left(\frac{\partial K^{nn}}{\partial \psi} |\nabla \psi|^2 \psi + K^{nn} |\nabla \psi|^2 + \frac{1}{2} K^{nn} \psi \frac{\partial}{\partial \psi} |\nabla \psi|^2 \right) \overline{c} \; dA, \end{aligned} \tag{15}$$

so dispersion in stream coordinates depends on the cross gradient of the diffusivity and mean flow speed.

When the cross-gradient diffusivity K^{nn} is approximately uniform ($\partial_\psi K^{nn} \rightarrow 0$) then the cross-stream diffusivity is approximately

$$K^{nn} = \frac{1}{2} \frac{\partial_t < \psi^2 \overline{c} >}{< \left(|\nabla \psi|^2 + \frac{1}{2} \psi \frac{\partial}{\partial \psi} |\nabla \psi|^2 \right) \overline{c} >}. \tag{16}$$

If the curvature of the streamlines is small ($\psi \partial_\psi |\nabla \psi|^2 \rightarrow 0$), then the expression for K^{nn} reduces to

$$K^{nn} \approx \frac{1}{2} \frac{\partial_t < \psi^2 \overline{c} >}{< |\nabla \psi|^2 \overline{c} >}. \tag{17}$$

The $|\nabla\psi|^2$ factor in the denominator represents that the conversion between dispersion in ψ coordinates and length coordinates.

Finally note that if the center of mass of the tracer in streamline coordinates is not at $\psi = 0$, i.e. $< \psi\overline{c} > \neq 0$, then the dispersion must be calculated as the growth rate of the centered second moment.

b. *Estimates of tracer dispersion across streamlines in the Drake Patch*

We introduced three different estimators of σ_y^2 in latitude coordinates in Section 4a. We now compare those estimates to equivalent ones in streamline coordinates to test whether the assumption that the flow in the DIMES region is zonal is sufficiently accurate for our calculations. We choose the time-mean surface geostrophic streamfunction $\psi = g\eta/f$, where g is the gravitational constant, η is sea surface height and f is the local Coriolis frequency, to define our streamlines. Fig. 12 shows estimates of K^{yy} (top) and K^{nn} (bottom) versus time using three methods: a second moment which assumes all datapoints are independent, a binned second moment averages along the stream (zonally) within cross-stream (meridional) bins, and a least-squares fit to a Gaussian distribution using the binned data (left to right). To define the streamlines, the model's sea surface height was averaged from year 5 to 10, then coarse-grain averaged using a Shapiro (1970) filter to remove eddy aliasing. In order to smooth the diffusivity in time, we plot the time-integrated rate of dispersion $K^{yy} = \sigma_y^2/2t$ rather than the instantaneous rate of dispersion defined in Eq. (5). As the tracer enters the Drake Passage, the streamlines bend and turn northward. This turning northward artificially increases K^{yy} and the bending would make the curvature term in the denominator of Eq. (16) significant. Also, the narrowing of the stream in and downstream of the Drake Passage likely invalidates the assumption that $\partial_\psi K^{nn} \rightarrow 0$. To alleviate all of these issues we have restricted the tracer dispersion calculations shown in Fig. 12 to tracer that is west of 75°W), which encompasses nearly all of the tracer shown in Fig. 1 at t =1 year.

In the left panels of Fig. 12, the dispersion is integrated exactly as defined in the equations above. In the middle panels, meridional and cross-stream bins of equal width (25 bins, $1/2$ of a degree apart in latitude from 65°S to 53°S), and an equivalent bin width in ψ of approximately

4×10^3 m^{2}s^{-1}) are defined to bin the tracer before summing over across the stream. This calculation is essentially identical to the method on the left, but with less cross-stream resolution. In the right panels, the tracer is first binned as in the middle panels and then fitted to a meridional or cross-stream Gaussian profile via least-squares gradient descent, analogously to the method used in Ledwell et al. (1998). Fig. 12 shows that the three methods shown agree with each other when the full (upstream) tracer is taken into account, and that the latitudinal and cross-stream diffusivities are both approximately $K = 800 - 900$ m^{2}s^{-1} in the model at $t = 1$ year. When the full tracer is known, the estimates on the right agree with the estimates on the left in the ensemble mean (thick black line), but there is more uncertainty in the ensemble members (thin gray lines). The middle and left plots also decrease at later times as more of the tracer approaches the Drake Passage where the stream is slightly narrower, while this effect seems to be absent in the least-squares fits on the right.

Fig. 13 shows the same model estimates as Fig. 12 except considering only tracer at the locations sampled during the US2 cruise. The simplest diagnostic, on the left, equally weights each sample point by the amount of tracer there. This metric consistently underestimates the spread of the tracer because the US2 track has limited meridional extent and a bias towards sampling more near the center of mass of the tracer. However the spread amongst the ensemble members is tightest in the leftmost panels, and the decrease with time is monotonic, as it is when considering the full tracer in the left panels in Fig. 12. Thus we will use the second-moment metric (left panels) to extrapolate observed values of tracer concentration on the US2 cruise grid (see Section refestimatekappa).

The right panels of Fig. 13 show least-squares fits of the sub-sampled tracer to Gaussians distributions. This method is well-justified in the vertical where the tracer distribution is well-sampled and known to be Gaussian, but laterally the tracer may not be Gaussian, particularly if it contains filaments or has reached the SAF or PF, where K is likely not constant. Also, if the tracer distribution extends beyond the area bounded by the US2 cruise track then the least-squares approach can become unstable and fail to converge. The least-squares method accurately estimates the full dispersion shown in Fig. 12 up until day 400, but limitations are observed when

extrapolating the sub-sampled dispersion in Fig. 13. At early times ($t < 200$ days), the fits may be inaccurate because tracer is not well-distributed amongst the bins. At intermediate times ($200 < t < 400$ days), the scatter amongst ensemble members is more than a factor of two. Finally, at times longer than 400 days the extrapolated values in Fig. 13 diverge in y, but not in ψ, from the values in Fig. 12.

c. *Estimates of tracer dispersion across streamlines in DIMES*

Fig. 13 further estimates of eddy diffusivity using the same three methods described in Section 4a, but using streamlines coordinates. The second moment of the tracer in streamline coordinates is estimated as $\sigma^2_\psi = \langle \psi^2 c \rangle / \langle |\nabla \psi|^2 c \rangle$ and data are averaged in streamline bins instead of latitude bins. We did not include the additional curvature terms, because they simply add noise to the estimates. The mean dynamic topography from AVISO (CNES-CLS09 Version 1.1, Rio et al. 2011) is used to define the streamfunction coordinate system. The estimates using streamfunction coordinates are slightly smaller for all methods, but the uncertainty range is larger. Estimates using streamfunction coordinates are similar to those obtained using latitude coordinates but somewhat smaller than latitude coordinates because the streamlines are not perfectly zonal and the tracer center of mass drifts south over the first year by about 0.5–0.75°. The uncertainty of the streamline estimates, however, is larger, because we rely on the surface streamfunction to infer the streamlines at 1500m depth and the calculation of $|\nabla \psi|^2$, which appears in the denominator of σ^2_ψ, is quite noisy.

APPENDIX B

Model setup and comparison with hydrography

The Drake Patch model is a regional configuration of the MITgcm, on a 1/20th of a degree resolution latitude-longitude grid. Horizontal vorticity is advected with a forth-order accurate spatial discretization using an enstrophy conserving (Arakawa and Lamb 1977) and vector invariant formulation. Horizontal viscosity is biharmonic, with an amplitude that scales according to local grid spacing and stresses (Fox-Kemper and Menemenlis 2008). Vertical viscosity is Laplacian and a quadratic bottom drag is imposed in the lowest layer. Momentum, temperature and salinity is forced at the surface by re-analysis from the European Centre for Medium Range Weather Forecasts (ECMWF ERA-Interim) on a 6-hourly timescale and at approximately 0.7 degree resolution (Dee et al. 2011). The initial hydrography is taken from an average of OCCA's December 2004 and January 2005 fields. There is dynamic sea ice and the freezing temperature is set to $T = 273.2501 - 0.0575 \cdot S$. Advection of temperature, salinity and passive tracers is by a spatially seventh-order accurate, monotonicity preserving scheme (Daru and Tenaud 2004). The K-profile parameterization scheme of Large et al. (1994) is used to parameterize vertical mixing due to boundary layer shear and convective instability. Table 4 summarizes the numerical parameters. The bathymetry was downloaded from `ftp://topex.ucsd.edu/pub/srtm30_plus/topo1_topo2/topo1.grd` and is David Sandwell's SRTM30_PLUS V7 averaged to 1/20$^{\text{th}}$ of a degree from 1-minute. Lateral boundary conditions (U, V, S, T, and sea ice) on a monthly time scale and one degree resolution from OCCA are interpolated onto the model's resolution. A relaxation boundary condition absorbs outgoing flow over a one degree sponge layer (see Section 6.3.2 of MITgcm Group 2011, for details of the MITgcm's relaxing boundary condition scheme). The model includes the MITgcms sea-ice thermodynamic model with standard settings (Losch et al. 2010). Bulk formulae are used to compute the atmospheric heat and fresh water flux data from the changing sea surface temperature (Large and Yeager 2004).

a. *Comparison of Drake Patch model against hydrography*

Fig. 14 compares the model's hydrography (right plots) with WOCE CTD data (left plots) from sections P18 (top), P19 (middle), and A21 (bottom), which are denoted with gray dashed lines in Fig. 3. The westernmost section, P18 at 103°W, is in a relatively quiescent region of the ACC,

near the initial DIMES tracer injection point US1. The SAF is visible at (103°W, 55°S) and PF at (103°W, 60°S) in both the model and in WOCE P18. North of 60°S there appears to be a deeper mixed layer, or mode water, in the model compared to observations. Deeper model mixed layers are expected because the model does not have a submesoscale parameterization for mixed layer restratification (Fox-Kemper and Ferrari 2008). At P19 (88°W), the model appears to be have more eddy activity south of 60°S than the observations. There is also more mode water present at P19 in the model than in observations. Within the Drake Passage, at Section A21, the SAF appears similar between the model and observations, but the PF is stronger in the model and displaced northwards by about half a degree. There also appears to be a bowl of low density water in the model between 60°S and 58°S, which does not appear in the observations below 1 km. The bowl of low density water in the model likely results from the path of the ACC in the model along A21, visible in Fig. 3b. The transect appears to run almost parallel to the jet at 58.5°S.

b. *Vertical diffusivity in the model*

Ledwell et al. (2011) showed that diapycnal diffusivity upstream of the Drake Passage is approximately 1.3×10^{-5} m^{2}s^{-1} at 1500 m depth. However many eddying z-coordinate coordinate models contain a horizontal bias as isopycnal surfaces become steeply inclined, which can lead to numerically generated diapycnal mixing of the order of 10^{-4} m^{2}s^{-1} (Griffies et al. 2000). Hill et al. (2012) show that this spurious diapycnal mixing can be limited to $K^z < 10^{-5}$ m^{2}s^{-1} when the vertical tracer variations are well-resolved and a second order moment (SOM) advection scheme (Prather 1986) is employed. Specifically, for a tracer with a Gaussian concentration and a vertical half-width of 50 m and layer thicknesses of 10 m, they obtain a diapycnal diffusivity of about 0.5×10^{-5} m^{2}s^{-1} using the SOM scheme with a flux limiter (their simulation A2). However when the Gaussian profile is not well resolved, *i.e.,* layer thicknesses of 100 m, the flux limited scheme produces 8 times more diapycnal diffusivity. Without a flux limiter (simulation A1) the diffusivity stays under 10^{-5} m^{2}s^{-1}.

Fig. 15 shows the evolution of tracer variance in density space in the Drake Patch model for a single tracer released with a Gaussian initial profile with half-width $\sigma_z = 75$ m, using the SOM

advection scheme without flux limiter and a 7th-order, one-step, monotonicity preserving method (Daru and Tenaud 2004). All layers shallower than 2km in the Drake Patch are thinner than 35 m, so this tracer, centered at 1500 m is well resolved in the vertical. Converting from variance in density coordinates to height coordinates using the average neutral density gradient at 1500m as $d\rho^n/dz \approx -2600^{-1}$kg m^{-4} yields $K^z < 10^{-5}$ m^{2}s^{-1} for both advection schemes.

References

Abernathey, R. P., D. Ferreira, and A. Klocker, 2013: Diagnostics of eddy mixing in a circumpolar channel. *Ocean Modell.*, Submitted.

Abernathey, R. P., J. Marshall, and D. Ferreira, 2011: The dependence of Southern Ocean meridional overturning on wind stress. *J. Phys. Oceanogr.*, **41**, 2261–2278, doi:10.1175/JPO-D-11-023.1.

Abernathey, R. P., J. Marshall, and M. Mazloff, 2010: Enhancement of mesoscale eddy stirring at steering levels in the Southern Ocean. *J. Phys. Oceanogr.*, **40**, 170–184, doi:10.1175/2009JPO4201.1.

Arakawa, A. and V. Lamb, 1977: Computational design of the basic dynamical processes of the UCLA general circulation model. *Methods in Computational Physics*, Academic Press, volume 17, 174–267.

Bretherton, F. P., 1966: Critical layer instability in baroclinic flows. *Quart. J. Roy. Meteor. Soc.*, **92**, 325–334.

Daru, V. and C. Tenaud, 2004: High order one-step monotonicity-preserving schemes for unsteady compressible flow calculations. *J. Comput. Phys.*, **193**, 563–594.

Dee, D. P., S. M. Uppala, A. J. Simmons, P. Berrisford, P. Poli, S. Kobayashi, U. Andrae, M. A. Balmaseda, G. Balsamo, P. Bauer, P. Bechtold, A. C. M. Beljaars, L. van de Berg, J. Bidlot, N. Bormann, C. Delsol, R. Dragani, M. Fuentes, A. J. Geer, L. Haimberger, S. B. Healy, H. Hersbach, E. V. Hlm, L. Isaksen, P. Kllberg, M. Khler, M. Matricardi, A. P. McNally, B. M. Monge-Sanz, J.-J. Morcrette, B.-K. Park, C. Peubey, P. de Rosnay, C. Tavolato, J.-N. Thpaut, and F. Vitart, 2011: The ERA-Interim reanalysis: configuration and performance of the data assimilation system. *Quart. J. Roy. Meteor. Soc.*, **137**, 553–597, doi:10.1002/qj.828.

Ferrari, R. and M. Nikurashin, 2010: Suppression of eddy diffusivity across jets in the Southern Ocean. *J. Phys. Oceanogr.*, **40**, 1501–1519, doi:10.1175/2010JPO4278.1.

Firing, Y. L., T. K. Chereskin, and M. R. Mazloff, 2011: Vertical structure and transport of the Antarctic Circumpolar Current in Drake Passage. *J. Geophys. Res.*, **116**, C08015, doi:10.1029/2011JC006999.

Forget, G., 2009: Mapping ocean observations in a dynamical framework: a 2004-2006 ocean atlas. *J. Phys. Oceanogr.*, **39**, doi:DOI: 10.1175/2009JPO4043.1.

Fox-Kemper, B. and R. Ferrari, 2008: Parameterization of mixed layer eddies. part ii: Prognosis and impact. *J. Phys. Oceanogr.*, **38**, 1166–1179.

Fox-Kemper, B. and D. Menemenlis, 2008: Can large eddy simulation techniques improve mesoscale rich ocean models? *Ocean Modeling in an Eddying Regime*, M. Hecht and H. Hasumi, eds., American Geophysical Union, volume 177, 319–338.

Gent, P. R. and J. C. McWilliams, 1990: Isopycnal mixing in ocean circulation models. *J. Phys. Oceanogr.*, **20**, 150–155.

Green, J. S. A., 1970: Transfer properties of the large-scale eddies and the general circulation of the atmosphere. *Quart. J. Roy. Meteor. Soc.*, **96**, 157–185.

Griffies, S. M., 2004: *Fundamentals of Ocean Climate Models*. Princeton University Press, Princeton, 1st edition.

Griffies, S. M., R. C. Pacanowski, and R. W. Hallberg, 2000: Spurious dyapycnal mixing associated with advection in a z-coordinate ocean model. *Mon. Wea. Rev.*, **128**, 538–564.

Hill, C., D. Ferreira, J.-M. Campin, J. Marshall, R. Abernathey, and N. Barrier, 2012: Controlling spurious diapycnal mixing in eddy resolving height-coordinate ocean models-insights from virtual deliberate tracer release experiments. *Ocean Modell.*, **45–46**, 14–26, doi:10.1016/j.ocemod.2011.12.001.

Ho, D. T., J. R. Ledwell, and W. M. Smithie Jr., 2008: Use of SF_5CF_3 for ocean tracer release experiments. *Geophys. Res. Lett.*, **35**, L04602, doi:10.1029/2007GL032799.

Johnson, G. C. and H. L. Bryden, 1989: On the size of the Antarctic Circumpolar Current. *Deep-Sea Res.*, **36**, 39–53.

Killworth, P. D. and C. W. Hughes, 2002: Boundary conditions on quasi-stokes velocities in parameterizations. *J. Mar. Res.*, **60**, 19–45.

Klocker, A., R. Ferrari, and J. H. LaCasce, 2012a: Estimating suppression of eddy mixing by mean flows. *J. Phys. Oceanogr.*, **42**, 1566–1576.

Klocker, A., R. Ferrari, J. H. LaCasce, and S. Merrifield, 2012b: Reconciling float-based and tracer-based estimates of lateral diffusivities. *J. Marine Res.*, **70**, 569–602.

LaCasce, J. H., R. Tulloch, R. Ferrari, J. Marshall, D. Balwada, and K. Speer, 2013: Dimes floats diffusivity paper. *JPO*, **43**, to be submitted to *J . Phys. Oceanogr.*

Large, W., J. McWilliams, and S. Doney, 1994: Oceanic vertical mixing: A review and a model with nonlocal boundary layer parameterization. *Rev. Geophys.*, **32**, 363–403.

Large, W. and S. Yeager, 2004: Diurnal to decadal global forcing for ocean and sea-ice models: The data sets and flux climatologies. Technical report, NCAR, technical Report TN-460+STR.

Ledwell, J. R., L. C. St. Laurent, J. B. Girton, and J. M. Toole, 2011: Diapycnal mixing in the antarctic circumpolar current. *J. Phys. Oceanogr.*, **41**, 241–246, doi:10.1175/2010JPO4557.1.

Ledwell, J. R., A. J. Watson, and S. S. Law, 1998: Mixing of a tracer in the pycnocline. *J. Geophys. Res.*, **103**, 21499–21529.

Losch, M., D. Menemelis, J. M. Campin, P. Heimbach, and C. Hill, 2010: On the formulation of sea-ice models. part 1: Effects of different solver implementations and parameterizations. *Oceanogr. Meteor.*, **33**, 129–144.

Lu, J. and K. Speer, 2010: Topography, jets, and eddy mixing in the Southern Ocean. *JMR*, **68**, 479–502.

Marshall, J., A. Adcroft, C. Hill, L. Perelman, and C. Heisey, 1997a: A finite-volume, incompressible navier stokes model for studies of the ocean on parallel computers. *J. Geophys. Res.*, **102**, 5753–5766.

Marshall, J., C. Hill, L. Perelman, and A. Adcroft, 1997b: Hydrostatic, quasi-hydrostatic, and nonhydrostatic ocean modeling. *J. Geophys. Res.*, **102**, 5733–5752.

Marshall, J. and T. Radko, 2003: Residual-mean solutions for the ACC and its associated overturning circulation. *JPO*, **33**, 2341–2354.

Marshall, J., E. Shuckburgh, H. Jones, and C. Hill, 2006: Estimates and implications of surface eddy diffusivity in the Southern Ocean derived from tracer transport. *J. Phys. Oceanogr.*, **36**, 1806–1821.

Marshall, J. and K. Speer, 2012: Closure of the meridional overturning circulation through southern ocean upwelling. *Nat. Geosci.*, **5**, 171–180, doi:10.1038/ngeo1391.

Meredith, M. P., P. L. Woodworth, T. K. Chereskin, D. P. Marshall, L. C. Allison, G. R. Bigg, K. Donohue, K. J. Heywood, and C. W. Hughes, 2011: Sustained monitoring of the Southern Ocean at Drake Passage: past achievements and future priorities. *Rev. Geophys.*, **49**, RG4005, doi:10.1029/2010RG000348.

MITgcm Group, 2011: Mitgcm user manual, available online at `http://dev.mitgcm.org/public/r2_manual/latest/online_documents/manual.html`.

Naveira Garabato, A. C., R. Ferrari, and K. L. Polzin, 2011: Eddy stirring in the Southern Ocean. *J. Geophys. Res.*, **116**, C09019, doi:10.1029/2010JC006818.

Nikurashin, M. and R. Ferrari, 2011: Global energy conversion rate from geostrophic flows into internal lee waves in the deep ocean. *Geophys. Res. Lett.*, **38**, L08610, doi:10.1029/2011GL046576.

Nikurashin, M., G. K. Vallis, and A. Adcroft, 2013: Routes to energy dissipation for geostrophic flows in the Southern Ocean. *Nat. Geosci.*, **6**, 48–51, doi:10.1038/NGEO1657.

Nowlin, Jr., W. D., J. S. Bottero, and R. D. Pillsbury, 1982: Observations of the principal tidal currents at Drake Passage. *J. Geophys. Res.*, **87**, 5752–5770.

Phillips, H. E. and S. R. Rintoul, 2000: Eddy variability and energetics from direct current measurements in the Antarctic Circumpolar Current south of Australia. *J. Phys. Oceanogr.*, **30**, 3050–3076.

Pillsbury, R. D., T. Whitworth III, and W. D. Nowlin, Jr., 1979: Currents and temperatures as observed in Drake Passage during 1975. *J. Phys. Oceanogr.*, **9**, 469–482.

Plumb, R. A., 1986: Three-dimensional propagation of transient quasi-geostrophic eddies and its relationship with the eddy forcing of the time-mean flow. *J. Atmos. Sci.*, **43**, 1657–1678.

Prather, M., 1986: Numerical advection by conservation of second-order moments. *J. Geophys. Res.*, **91**, 6671–6681.

Redi, M. H., 1982: Oceanic isopycnal mixing by coordinate rotation. *J. Phys. Oceanogr.*, **12**, 1154–1158.

Rio, M. H., S. Guinehut, and G. Larnicol, 2011: New cnes-cls09 global mean dynamic topography computed from the combination of grace data, altimetry, and in situ measurements. *J. Geophys. Res.*, **116**, C07018, doi:10.1029/2010JC006505.

Russell, J. L., K. W. Dixon, A. Gnanadesikan, R. J. Stouffer, and J. R. Toggweiler, 2006: The southern hemisphere westerlies in a warming world: Propping open the door to the deep ocean. *J. Climate*, **19**, 6382–6390, doi:10.1175/JCLI3984.1.

Scott, R. B., J. A. Goff, A. C. Naveira Garabato, and A. J. G. Nurser, 2011: Global rate and spectral characteristics of internal gravity wave generation by gestrophic flow over topography. *J. Geophys. Res.*, **116**, C09029, doi:10.1029/2011JC007005.

Shapiro, R., 1970: Smoothing, filtering, and boundary effects. *Rev. Geophys.*, **8**, 359–387.

Simmons, A., S. Uppala, D. Dee, and S. Kobayashi, 2006: Era-interim: New ECMWF reanalysis products from 1989 onwards. *ECMWF Newsletter*, **110**, 25–35, available online at http://www.ecmwf.int/publications/newsletters/.

Smith, K. S. and J. Marshall, 2009: Evidence for enhanced eddy mixing at mid-depth in the Southern Ocean. *J. Phys. Oceanogr.*, **39**, 1037–1050.

Speer, K., S. R. Rintoul, and B. Sloyan, 2000: The diabatic Deacon cell. *JPO*, **30**, 3212–3222.

Stammer, D., 1998: On eddy characteristics, eddy transports, and mean flow properties. *J. Phys. Oceanogr.*, **28**, 727–739.

Treguier, A. M., 1999: Evaluating eddy mixing coefficients from eddy-resolving ocean models: A case study. *J. Marine Res.*, **57**, 89–108.

Tulloch, R. T., J. C. Marshall, C. Hill, and K. S. Smith, 2011: Scales, growth rates and spectral fluxes of baroclinic instability in the ocean. *J. Phys. Oceanogr.*, **41**, 1057–1076, doi:10.1175/2011JPO4404.1.

Young, W. R., 1981: *The vertical structure of the wind-driven circulation*. Ph.D. thesis, Massachusetts Institute of Technology.

Table 1: Brief information about the DIMES Cruises.

Cruise Code	Vessel	Cruise date	Days after release
US1	*RV Roger Revelle*	22 Jan to 18 Feb 2009	0
US2	*RV Thompson*	16 Jan to 23 Feb 2010	366
UK2	*James Clark Ross*	7 Dec to 5 Jan 2011	687
UK2.5	*James Clark Ross*	11–25 Apr 2011	797
US3	*RV Thompson*	13–18 Aug 2011	917

Table 2: Observed estimates of the average rate of dispersion of the DIMES tracer over the first year on the US2 cruise track ($\sigma^2(1year)/2years$ m^{2}s^{-1}). The 95% confidence intervals are determined using bootstrapping. The first three lines report estimates suing three different methods to estimate $\sigma^2(1year)$ in both latitude and streamline coordinates (see Section 4a and Appendix B). The last two rows report our best estimate of the diffusivity obtained by multiplying the first two rows by a model derived factor that accounts for the incomplete tracer sampling during the US2 cruise (see Section 4c). Bins of 1/2° width span from $65°$S to $53°$S in latitude coordinates, and from -1.75$\times 10^4$ m^{2}s^{-1} to 8×10^4 m^{2}s^{-1} in streamfunction coordinates.

Method	Latitude coordinates (y)	Stream coordinates (ψ)
Second moment	407 (323–495)	391 (227–558)
Binned second moment	524 (254–847)	476 (179–890)
Gaussian least-squares fit	708 (358–840)	665 (251–930)
Extrap. second moment	709$\pm$257	776$\pm$ 436
Extrap. binned second moment	648$\pm$428	664$\pm$ 520

Table 3: Modeled estimates of average rate of dispersion of the tracer ensemble over the first year using three methods and two coordinate systems ($\sigma^2(1year)/2years$ m^{2}s^{-1}). The mean value is based on the ensemble average tracer, while the upper and lower bounds (in brackets) are the maximum and minumum values from the 12 tracer release experiments. Estimates using the full tracer west of 75°W are in the top three rows and estimates using the subsampled tracer on the US2 grid are in the bottom three rows. Bins of 1/2° width span from $65°$S cto $53°$S in latitude coordinates, and from -1.75$\times 10^4$ m^{2}s^{-1} to 8×10^4 m^{2}s^{-1} in streamfunction space.

Method	Latitude coordinates (y)	Stream coordinates (ψ)
Full Second moment	888 (719–966)	903 (739–998)
Full Binned second moment	887 (717–967)	905 (743–1001)
Full Binned and least-squares fit	941 (672–1062)	1056 (816–1238)
US2 Second moment	510 (349–652)	455 (327–663)
US2 Binned second moment	717 (503–989)	649 (459–768)
US2 Binned and least-squares fit	968 (495–1474)	875 (472–1324)

Table 4: Numerical parameters used in the Drake Patch simulation.

Parameter	Value
Vertical viscosity (m^2s^{-1})	5.66×10^{-4}
Leith harmonic viscosity factor	1
Leith biharmonic viscosity factor	1.2
Vertical diffusivity (T,S) (m^2s^{-1})	1×10^{-5}
Side boundary	Free slip
Bottom boundary	No slip
Quadratic bottom drag (s^{-2})	2.5×10^{-3}
Time step (s)	120
Horizontal grid spacing (degrees)	0.05
Shear instability critical Richardson number	0.358

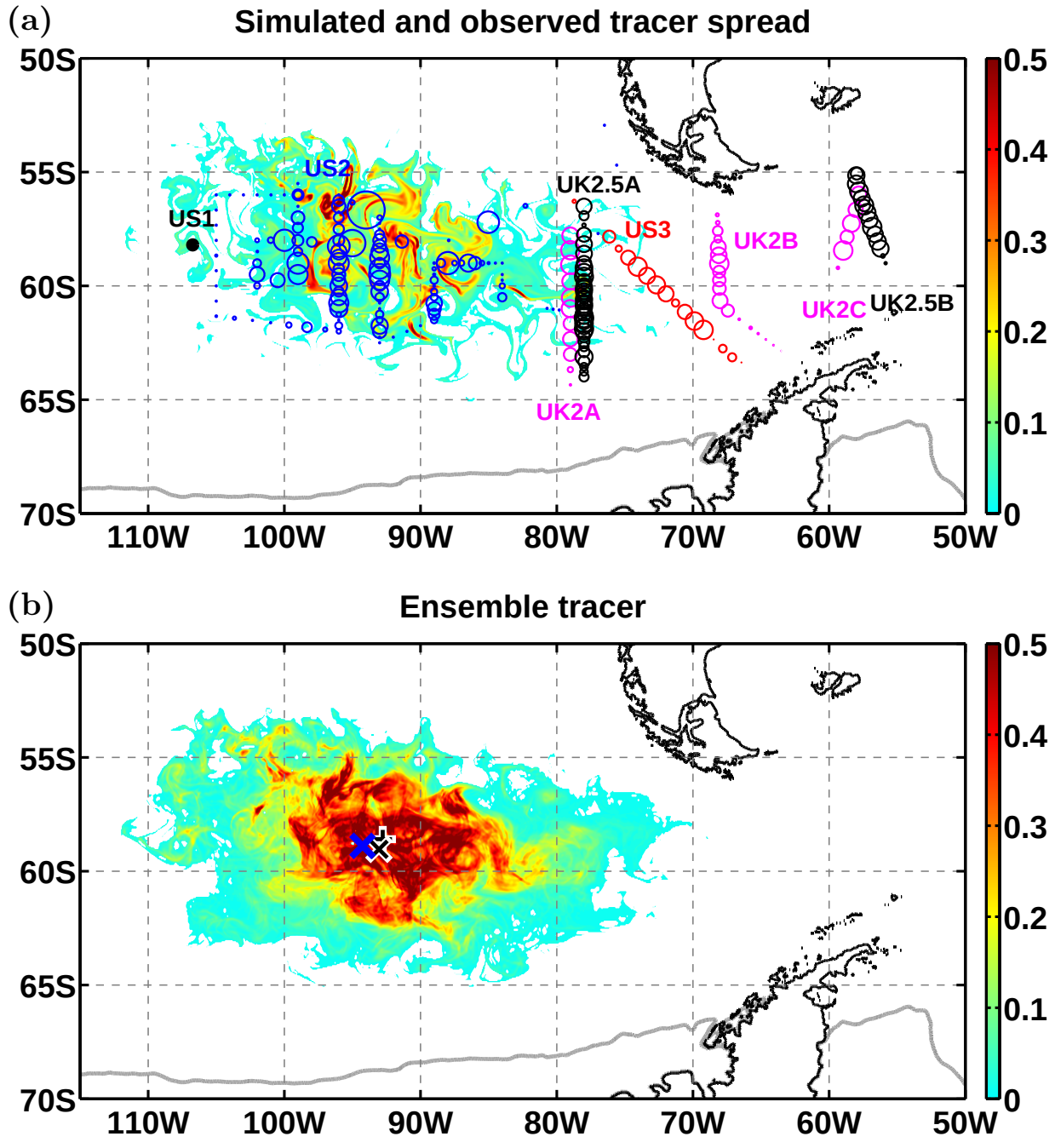

Figure 1: Caption next page.

Figure 1: (a) Map of DIMES tracer patch region showing the injection location (US1), and the column integrated tracer concentrations (circles) during subsequent cruises (US2, UK2, UK2.5, US3). The circle diameters are proportional to the tracer concentration. For each cruise the concentrations are normalized by the larger concentration found in that cruise. The contour plot in the background is the of the column integrated concentration of a modeled tracer 365 days after release (cyan-to-red colormap). The modeled tracer concentration is also normalized by its maximum, and values less than 0.01 are shaded white. The climatological mean of the modeled sea ice extent is shown as a gray line. (b) Snapshot of the column integrated concentration from the ensemble average of 12 tracer release experiments 365 days after release. The blue 'x' marks the location of the center of mass of the DIMES tracer sampled on the US2 grid one year after release. The black 'x' is the location of the center of mass of the modeled ensemble tracer sampled only on the US2 grid, and the black '+' (beneath the black 'x') is the location of the emsemble tracer's center of mass based on the full tracer distribution.

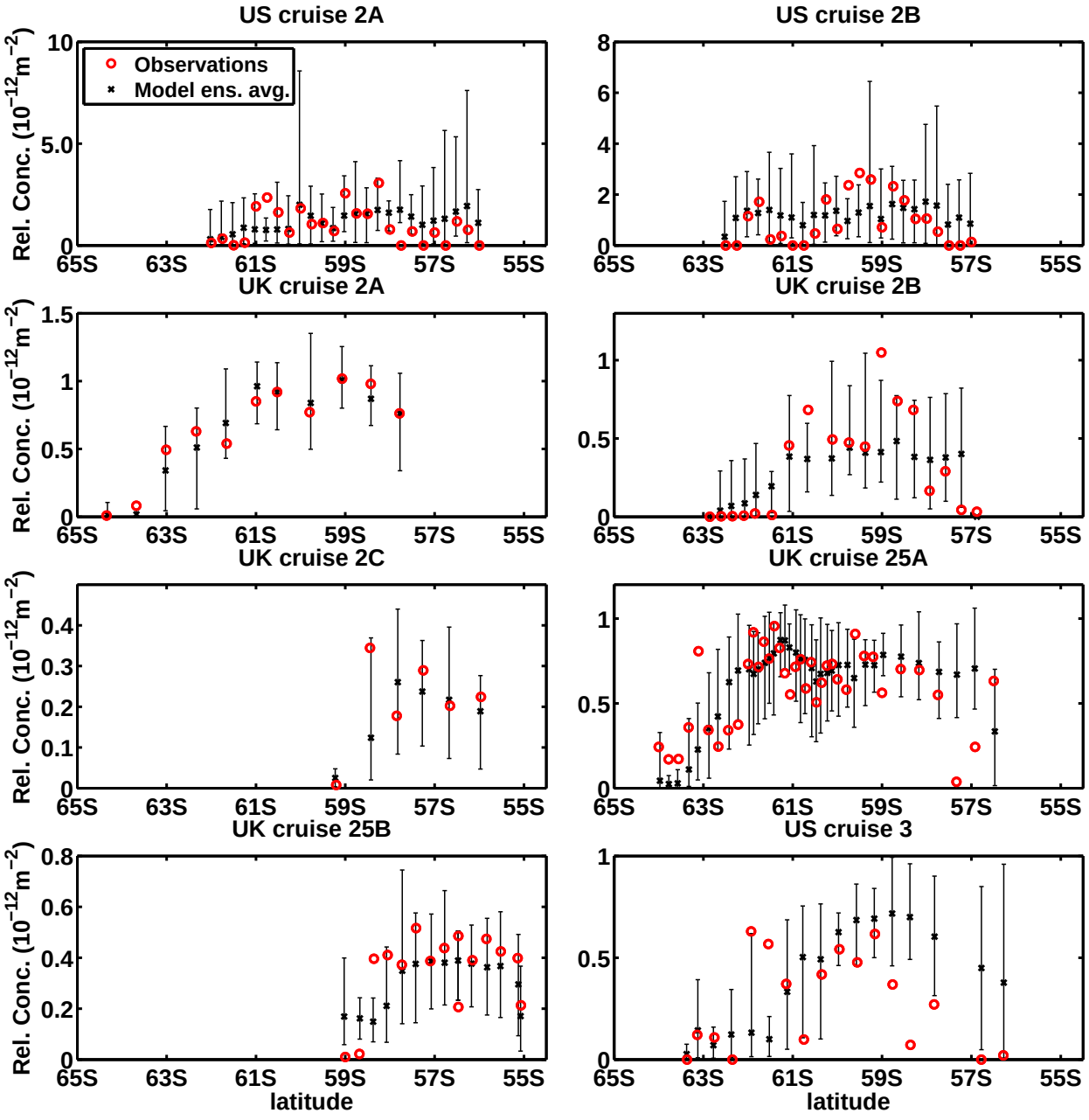

Figure 2: Observed (circles) and simulated (x's) column-integrated tracer concentrations relative to the total amount of tracer released (units are m^{-2}) measured at individual stations during the cruises listed in Table 1 and shown in Fig. 1. Only a subset of Cruise US2 is shown: US-2A is the latitudinal transect at 96° and US-2B is the latitudinal transect at 93°. The spread in the modeled ensemble mean concentrations, shown as think black lines, is based on the maximum and minimum concentrations at each point of all 12 release experiments.

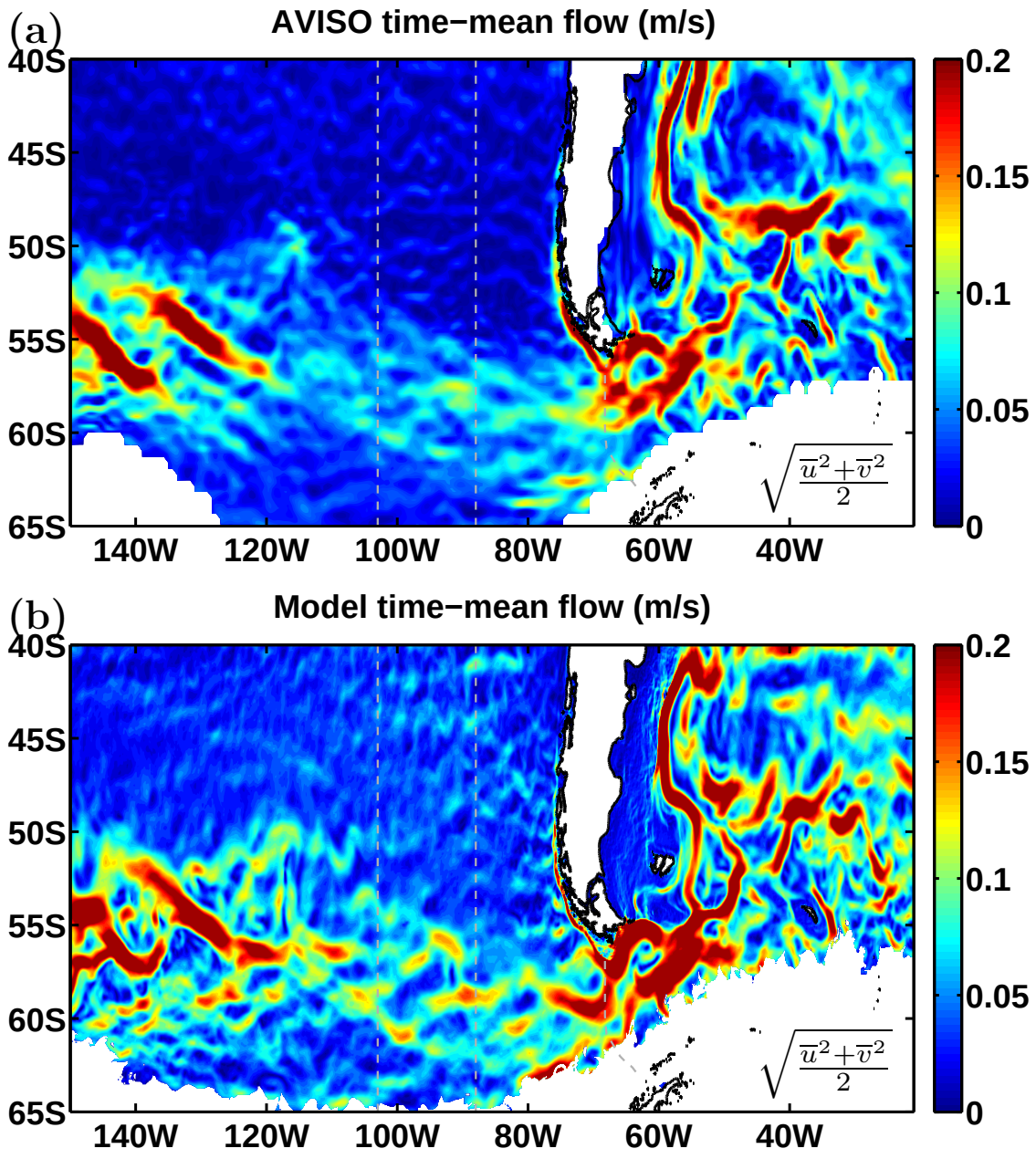

Figure 3: (a) Altimetry based (AVISO) time-mean geostrophic current speed averaged from 1993 to 2011. Regions around Antarctica where the AVISO data were missing sometime during the averaging period are left white. (b) Modeled time mean current speed averaged over model integration years 6, 7 and 8. White regions around Antarctica indicate maximum sea ice extent over the 3 year period. The two faint dashed lines are the locations of WOCE sections P18, P19, and A21 shown in Fig. 14.

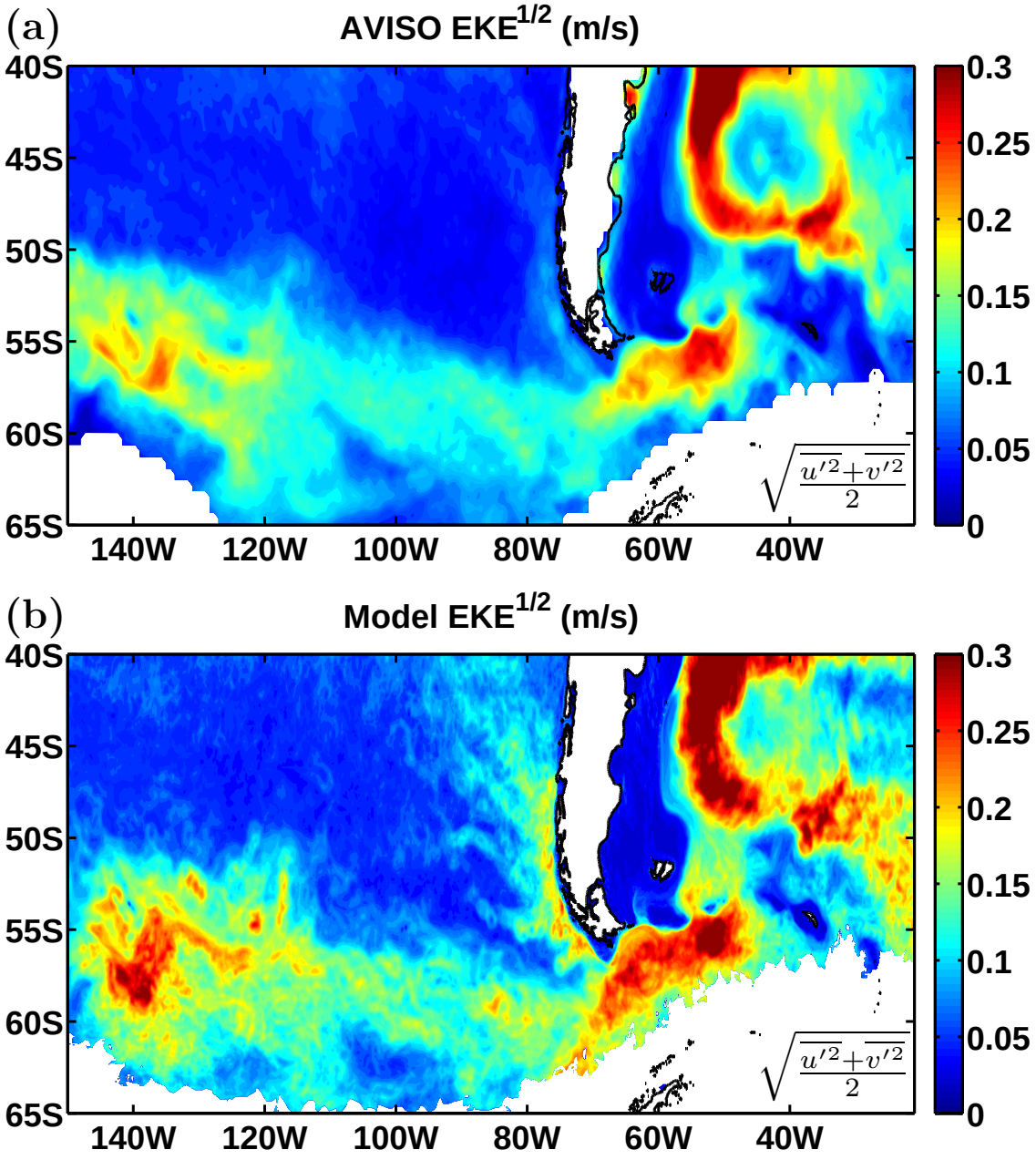

Figure 4: (a) AVISO geostrophic eddy current speeds ($EKE^{1/2}$) and (b) modeled eddy current speeds . The EKE is defined as the temporal fluctuation about the averages shown in Fig. 3.

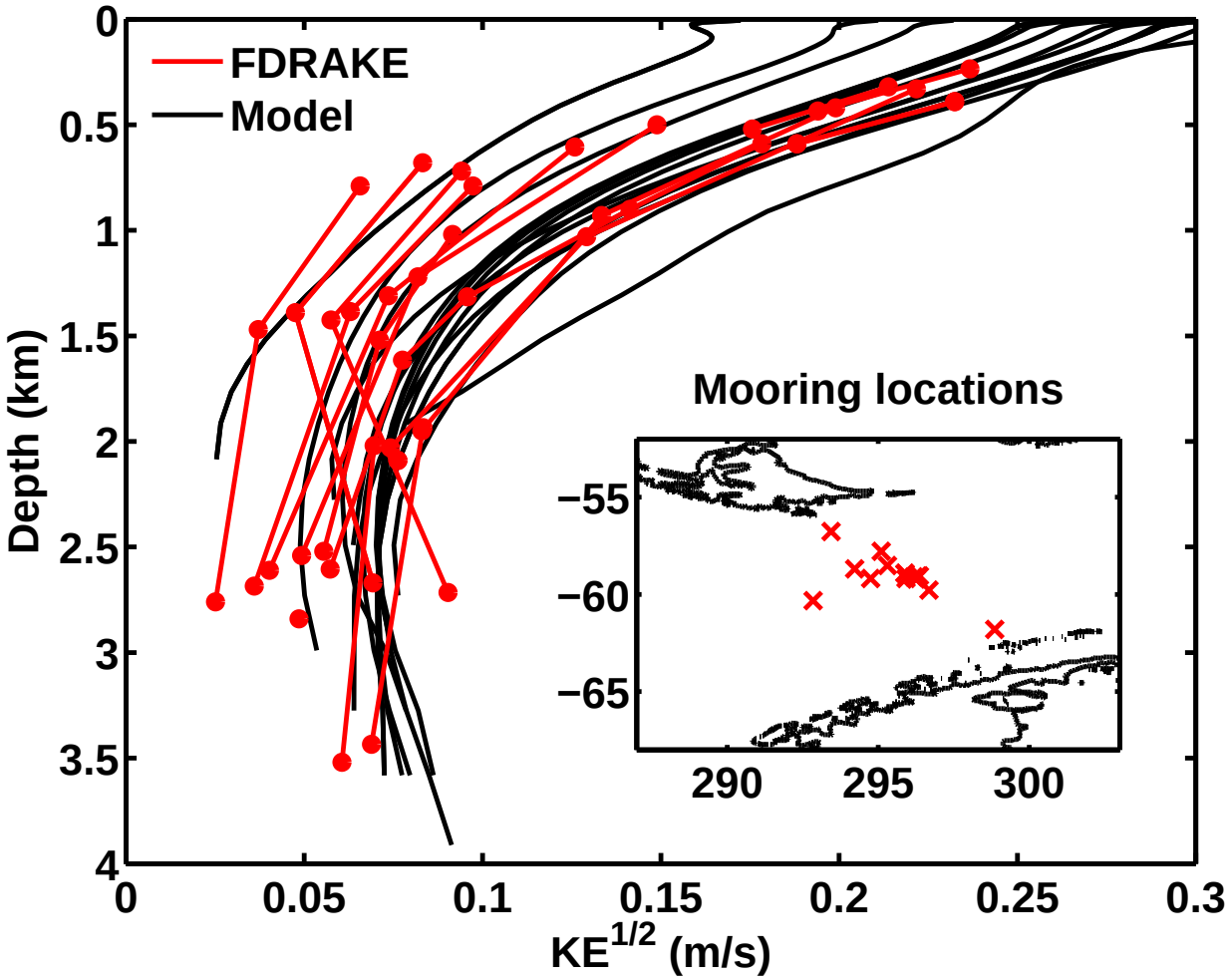

Figure 5: Comparison of simulated vertical structure of current speed ($KE^{1/2}$) (black lines) against FDRAKE mooring data from the late 1970's (red lines). The location of each FDRAKE mooring is plotted in the inset. The average length of the mooring data is 320 days. The black line with the largest EKE in the model is from the northernmost mooring location.

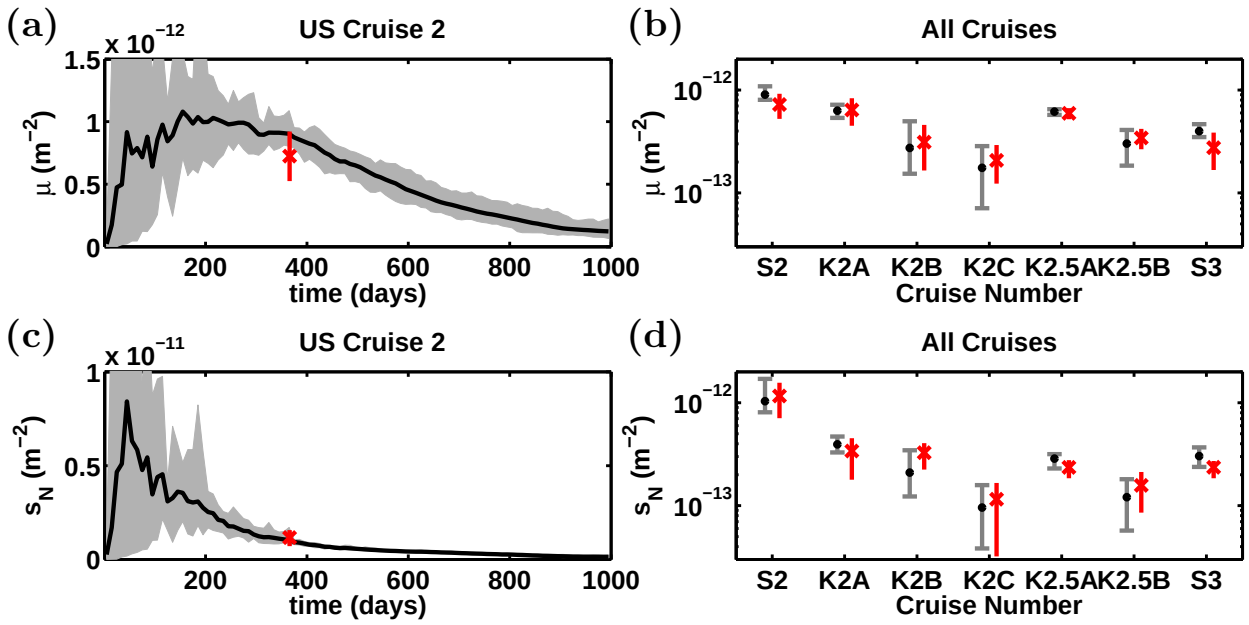

Figure 6: (a) Modeled average ($\mu = N^{-1}\sum c_i$) and (b) standard deviation ($s_N = \sqrt{(N-1)^{-1}\sum(c_i-\mu)^2}$) of the column integrated tracer concentration at the US2 cruise track locations versus time. The tracer concentrations are normalized by the total amount of tracer released, hence the units are m^{-2}. The red 'x' shows the observed tracer concentration and standard deviation from the DIMES US2 cruise, with the red line indicating a 95% confidence interval using bootstrapping. Gray shading indicates a the minimum and maximum values from the 12 tracer releases from the ensemble. (b) and (c) show the same means and standard deviations, but at the times of the cruises listed in Table 1 for the 4 DIMES cruises. he UK2 and UK2.5 cruises have been split into individual transects from west to east (K2A, K2B, K2C and K2.5A and K2.5B respectively. Notice that we used a logarithmic scale in these two panels, because the concentrations drop substantially in the subsequent cruises which were done two to three years after injection.

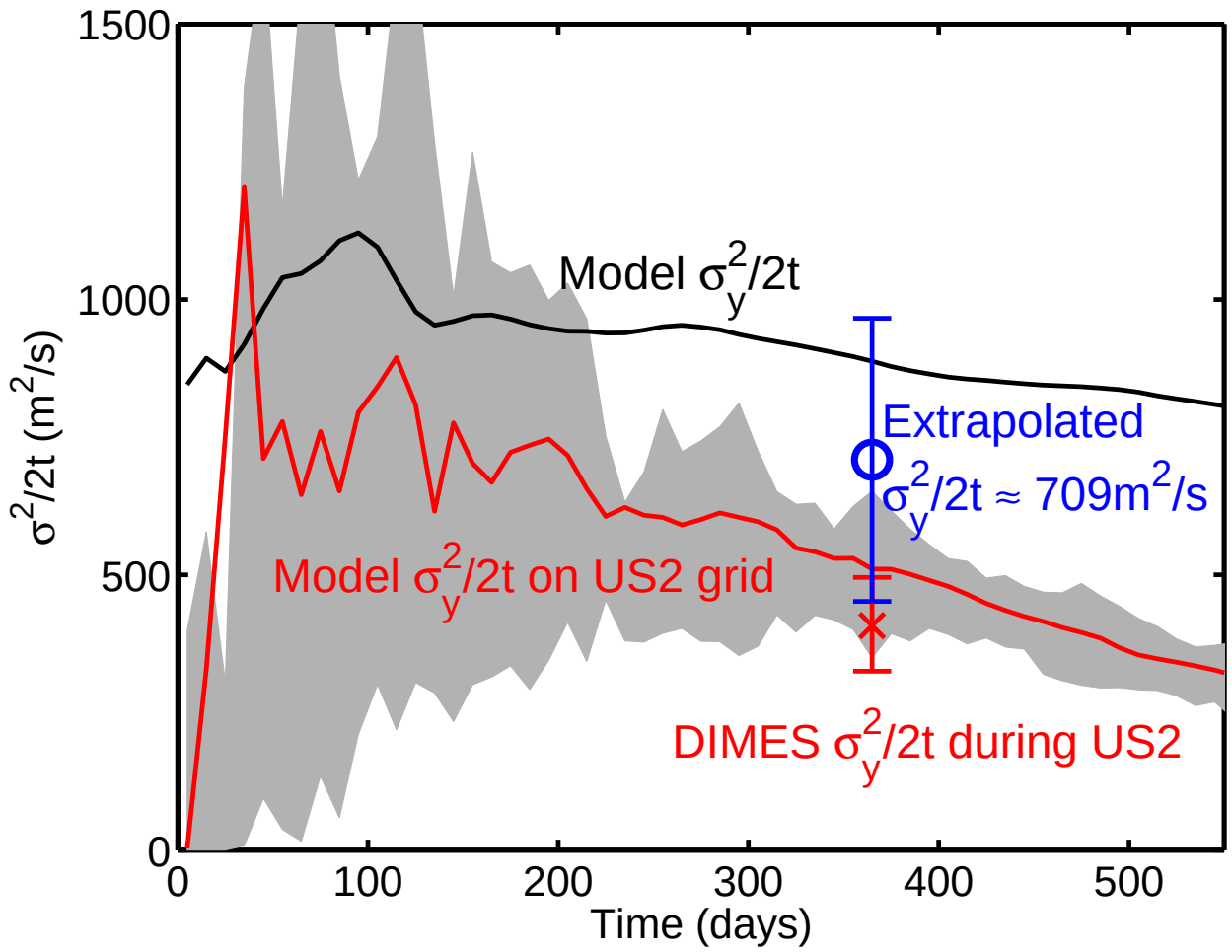

Figure 7: Comparison of the average rate of dispersion using: the full model ensemble average tracer (black line), the ensemble average tracer subsampled on the US2 cruise stations (red line with gray shading indicating the minima and maxima from the 12 release experiments), and the observed DIMES tracer during US2 (red 'x'). A 95% confidence interval on the DIMES tracer is estimated using bootstrapping. The blue circle and the blue error bar indicates the extrapolated estimate of the average rate of dispersion over the first year of the DIMES tracer using Eqs. 7 and 8.

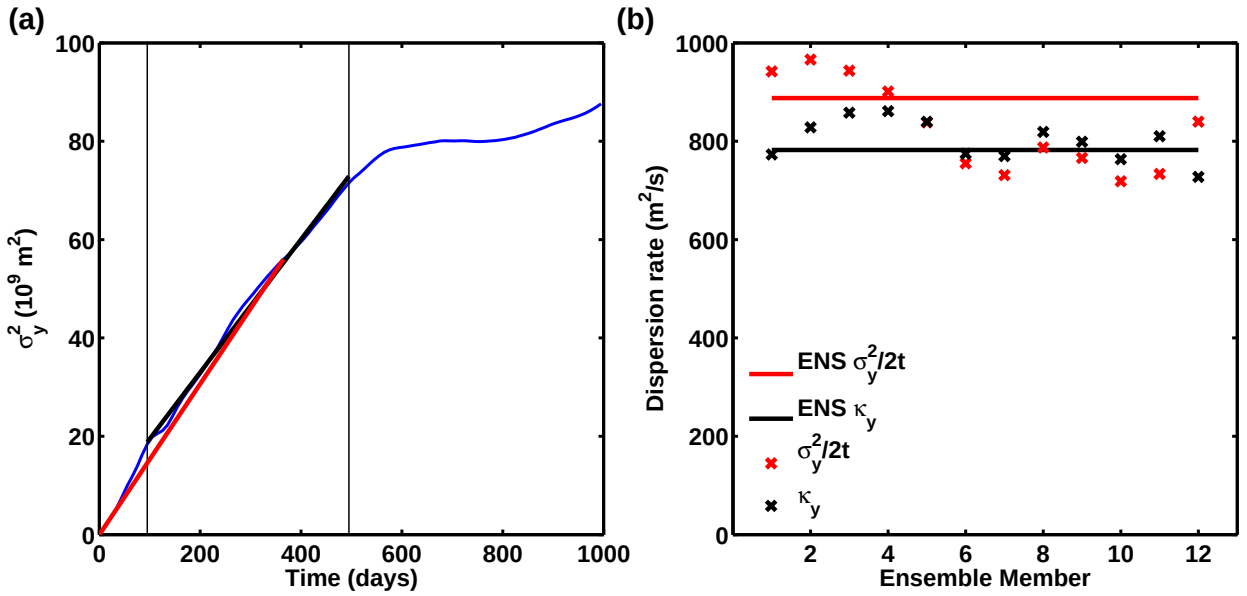

Figure 8: (a) Dispersion σ_y^2 of the ensemble mean tracer in the simulation versus time (blue line). The red line marks the average dispersion in the first year after release, with slope $\sigma_y^2(t)/2t$ where $t = 365$, and the black line marks a least-squares fit to the dispersion from $t = 100$ to $t = 500$. (b) The slopes of the red and black lines in (a) are plotted in (b) as solid red and black lines. The slopes each of each of the 12 tracer release experiments in the ensemble are plotted as red and black x's.

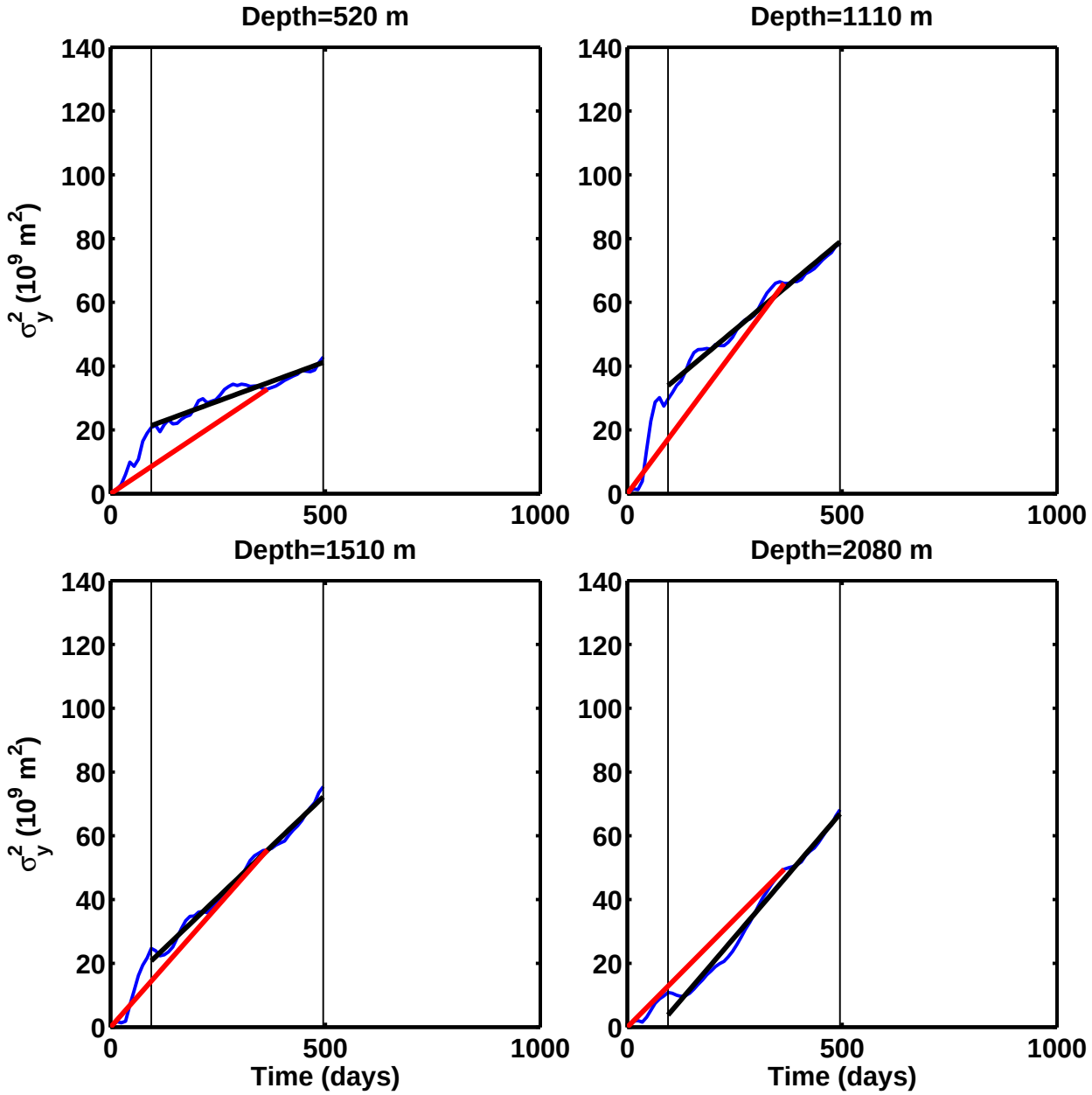

Figure 9: Dispersion σ_y^2 from model tracers released at four different depths at depths near 500 m, 1 km, 1.5 km, and 2 km (blue lines). The red lines are the average dispersion over the first year and the black lines are the least-squares fit dispersion between day 100 and day 500 as in Fig. 8.

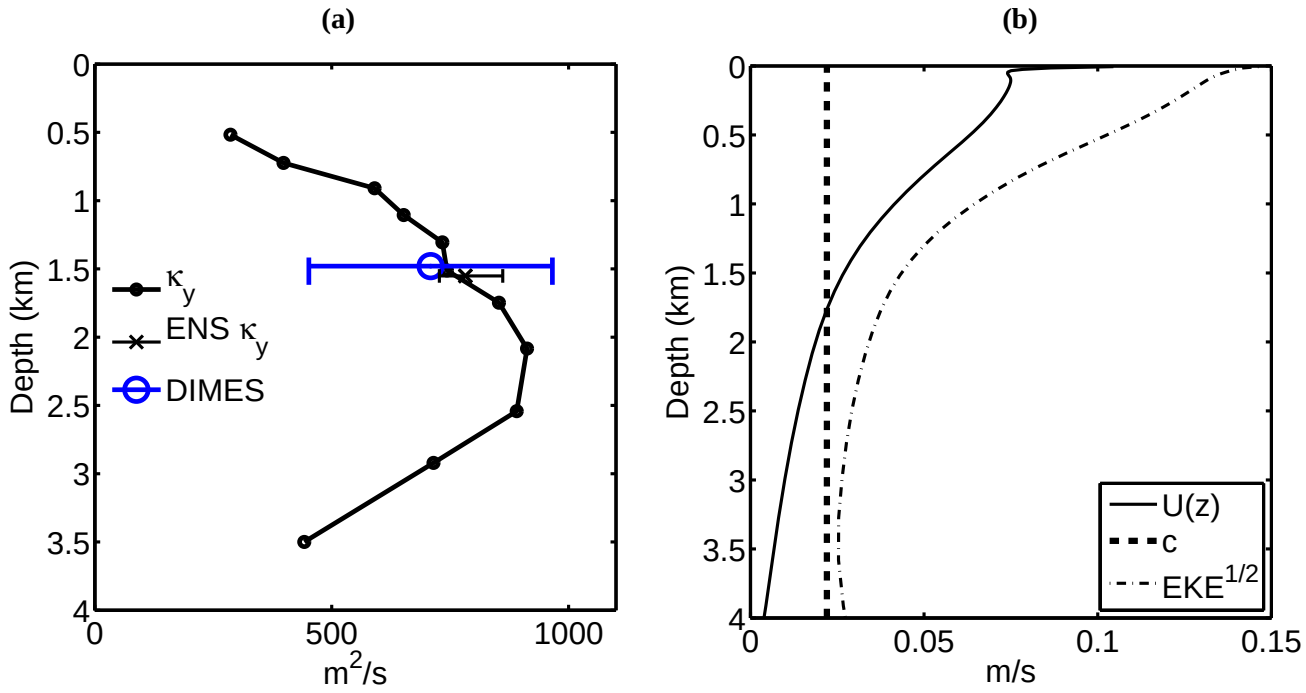

Figure 10: (a) Estimates of the vertical structure of the isopycnal eddy diffusivity upstream of 75°W at various depths. The eddy diffusivity is estimated as the least-squares fit dispersion between day 100 and day 500 (see Fig. FigDISP:fig). The estimates from the ensemble average tracer released at 1500m is indicated as a black 'x' with the error bar showing the minimum and maximum values from the 12 release experiments. (b) Model estimate of the mean flow, $U(z)$, eddy phase speed, c, and $EKE^{1/2}$, all averaged from 61°S to 56°S and 110°W to 80°W.

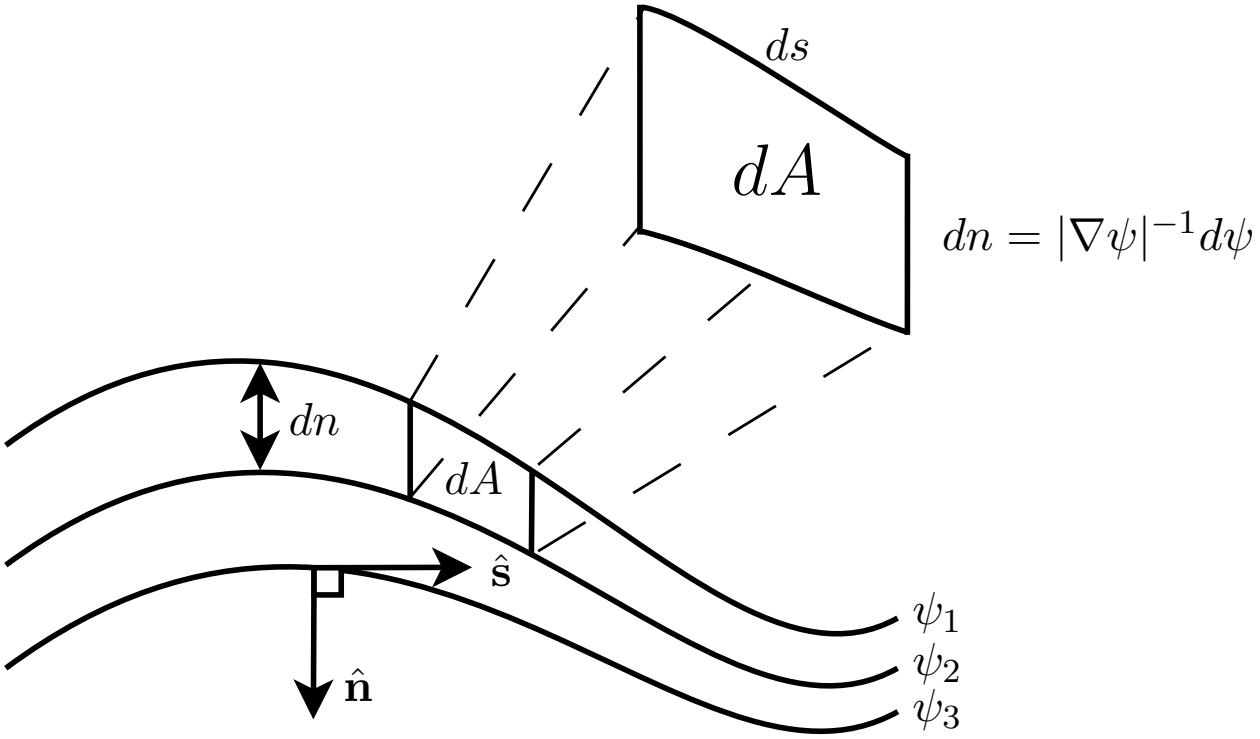

Figure 11: Streamline coordinate system. The s coordinate is along streamlines, the n coordinate in normal to it. The area of the patch A in streamline coordinate is indicated.

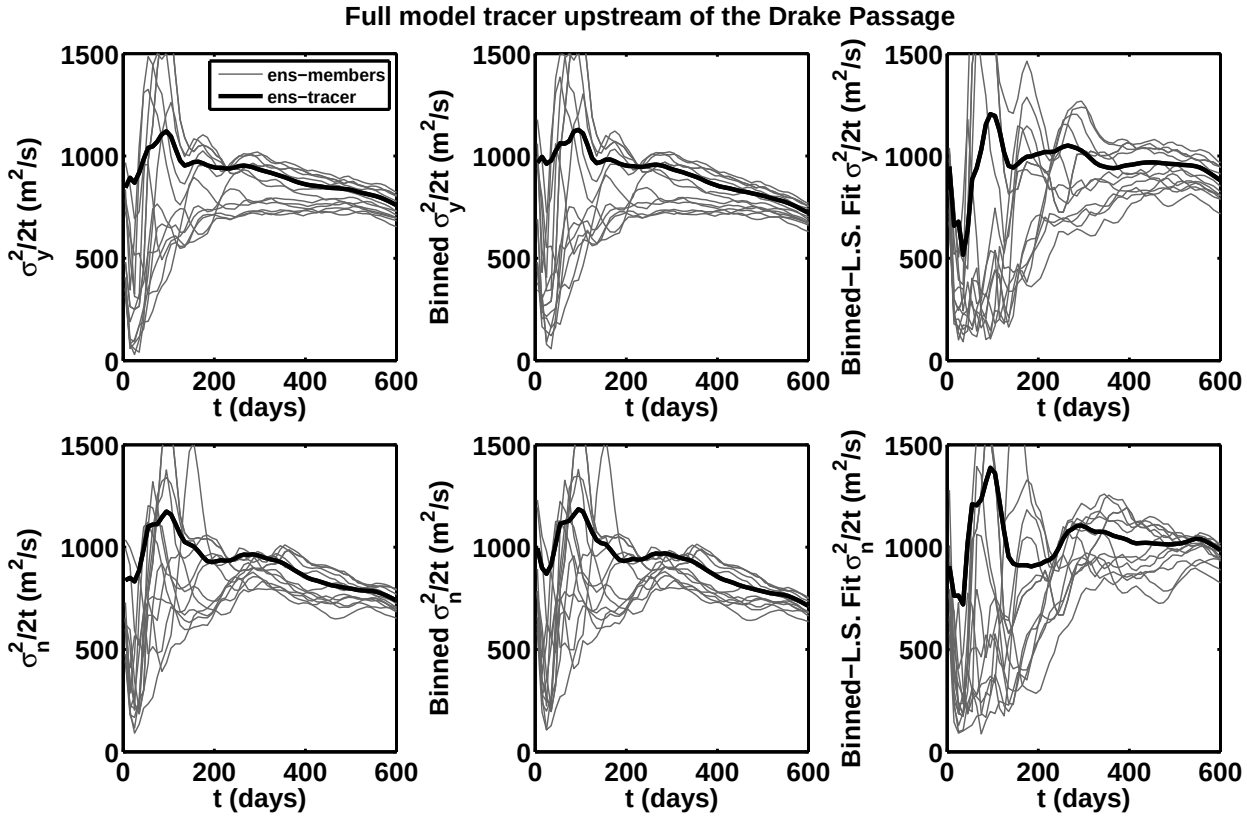

Figure 12: Three model based estimates (left to right) of eddy diffusivity at 1500m in latitude coordinates (top) and streamline coordinates (bottom). The eddy diffusivity is determined as the growth rate of the second moment of the tracer concentration. The three estimates of the second moment in latitude coordinates are: the second moment averaged over the whole area spun by the tracer $\sigma_y^2 =< y^2 c > / < c >$ (left), meridional binning followed by second moment $\sigma_y^2 = \sum y^2 \int c \, dx / \sum \int c \, dx$ (middle), and meridional binning followed by a least-squares fit to a Gaussian using gradient descent (right). The thick black line are estimated based on the ensemble average tracer $\overline{c}$, while the grey the gray lines are estimates based on the individual 12 tracer release experiments..

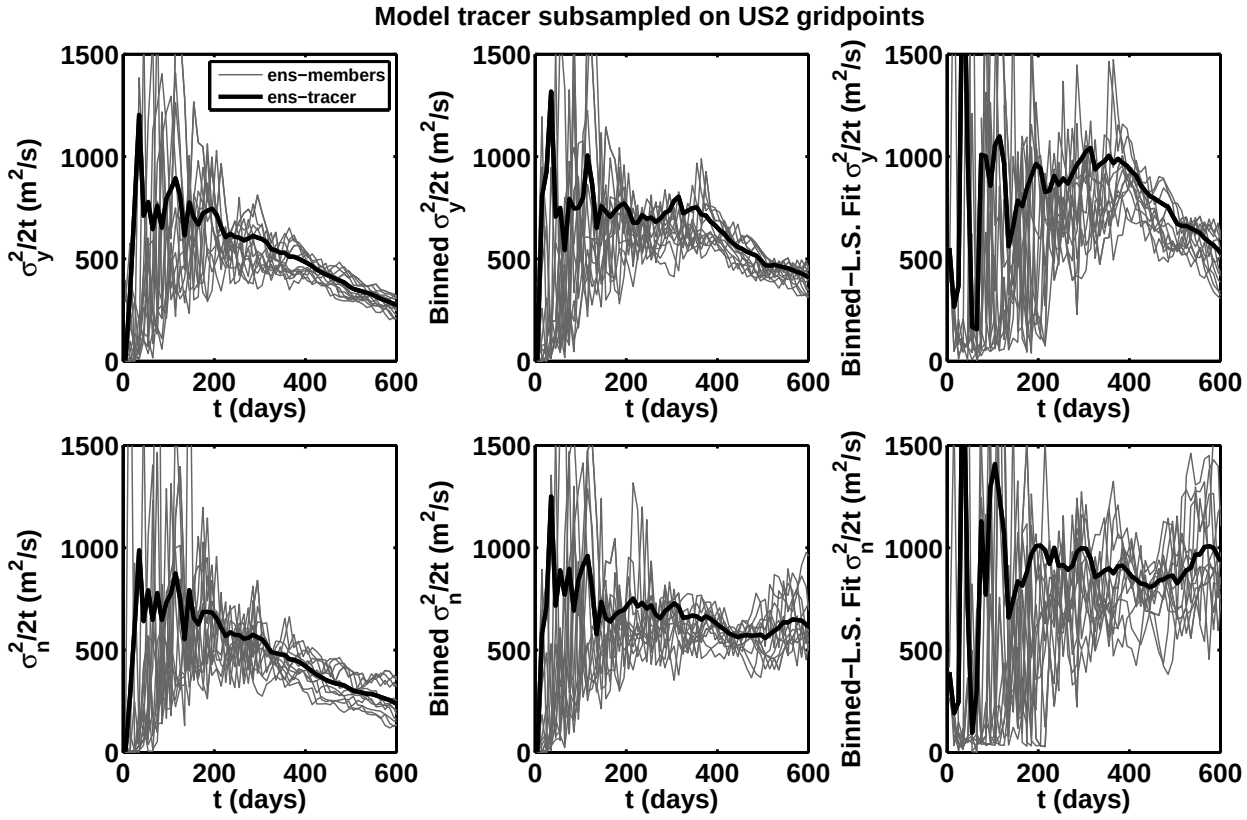

Figure 13: Three estimates (left to right) of diffusivity at 1500m in the model using tracer subsampled on the US2 cruise track locations, in latitude coordinates (top) and streamline coordinates (bottom). The eddy diffusivity is determined as the growth rate of the second moment of the tracer concentration. The three estimates of the second moment (in latitude coordinates) are: the second moment $\sigma_y^2 = \sum_i y_i^2 \overline{c}_i / \sum_i \overline{c}_i$ (left), meridionally binned second moment $\sigma_y^2 = \sum_j \left(y_j^2 \sum_i \overline{c}_i \right) / \sum_i \left(\sum_i \overline{c}_i \right)$ where j is a sum over bins and i is a sum over points within each bin (middle), a least-squares fit to a Gussian after binning meridionally.

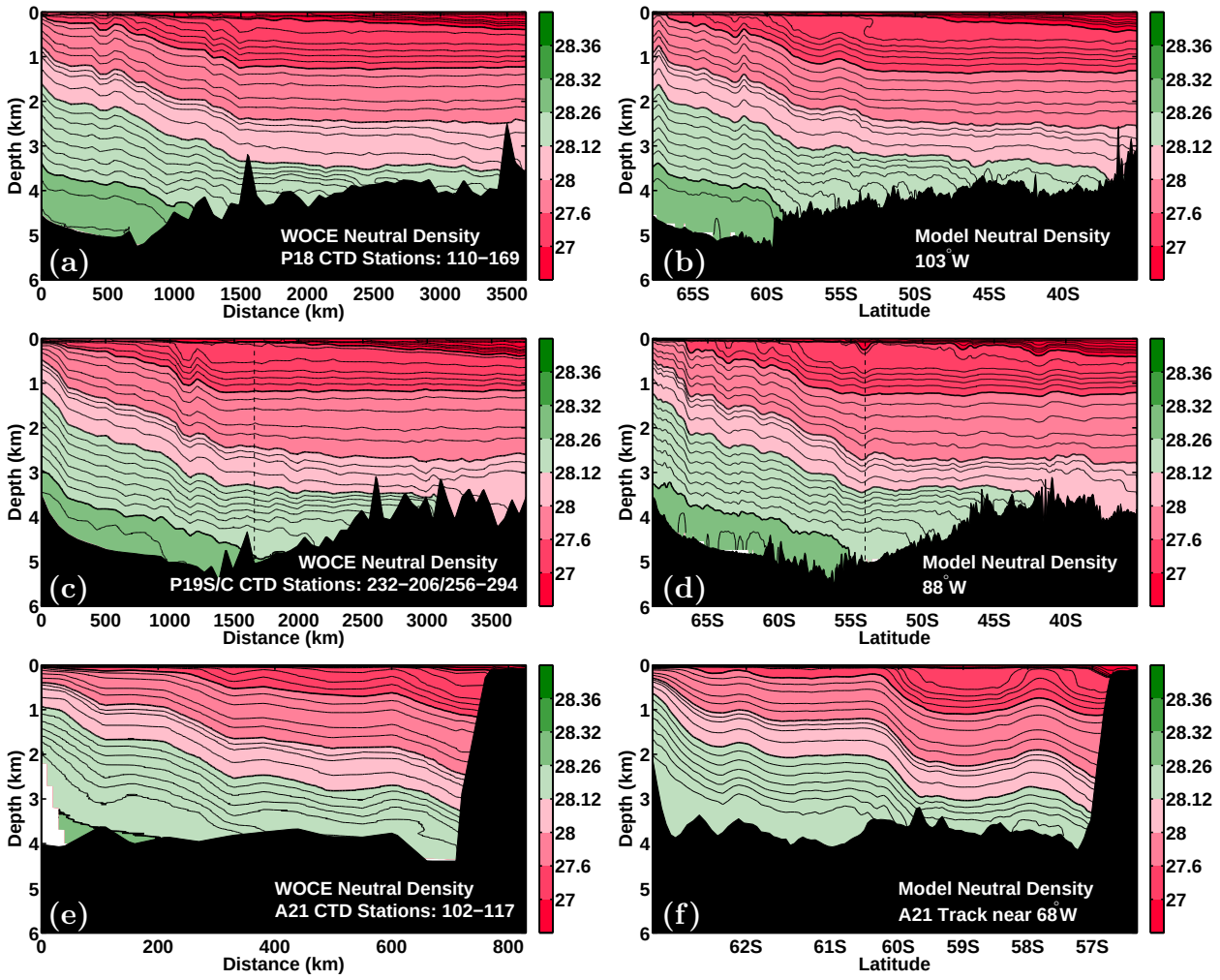

Figure 14: Comparison of WOCE (left) neutral density from Section P18 (top), P19 (middle), and A21 (bottom) with the Drake Patch model (right) at 103°W (top), 88°W (middle), and near (68°W,61°S) following A21 (bottom). The WOCE CTD profiles were collected in Early February 2008 (P18), January and March 1993 (P19) and late January 1990 (A21), and were plotted as a section using Delaunay triangulation with cubic interpolation. The modeled sections are snapshots on January 19 of the 6th year of integration for P18, the southern part of P19 and A21, and Feburary 18 for northern part of P19.

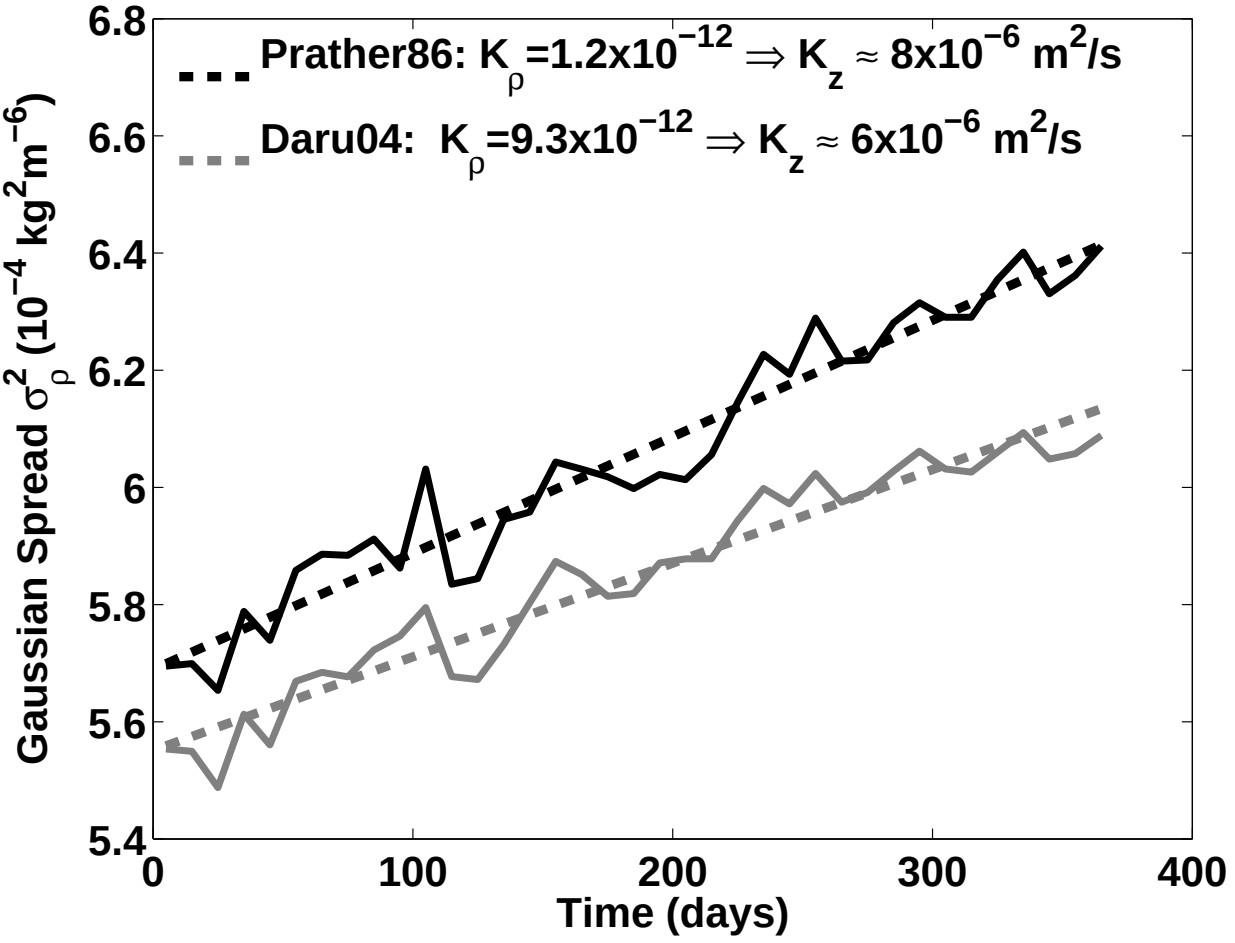

Figure 15: Time evolution of the variance of the tracer spread in density space for a tracer that was injected with a Gaussian concentration in the vertical, advected by advection schemes of Prather (1986) and Daru and Tenaud (2004). The squared half-width $\sigma_\rho(t)^2$ (indicated as continuous lines) is for a Gaussian fitted to the vertical profile of the tracer after integration along neutral density surfaces. A diapycnal eddy diffusivity is estimated as half the growth rate of $\sigma_\rho(t)^2$ (dashed lines). Converting into z-coordinates both schemes imply diapycnal mixing $K^z < 10^{-5}$ m^{2}s^{-1}.

Figure Captions

Fig. 1: (a) Map of DIMES tracer patch region showing the injection location (US1), and the column integrated tracer concentrations (circles) during subsequent cruises (US2, UK2, UK2.5, US3). The circle diameters are proportional to the tracer concentration. For each cruise the concentrations are normalized by the larger concentration found in that cruise. The contour plot in the background is the of the column integrated concentration of a modeled tracer 365 days after release (cyan-to-red colormap). The modeled tracer concentration is also normalized by its maximum, and values less than 0.01 are shaded white. The climatological mean of the modeled sea ice extent is shown as a gray line. (b) Snapshot of the column integrated concentration from the ensemble average of 12 tracer release experiments 365 days after release. The blue 'x' marks the location of the center of mass of the DIMES tracer sampled on the US2 grid one year after release. The black 'x' is the location of the center of mass of the modeled ensemble tracer sampled only on the US2 grid, and the black '+' (beneath the black 'x') is the location of the emsemble tracer's center of mass based on the full tracer distribution.

Fig. 2: Observed (circles) and simulated (x's) column-integrated tracer concentrations relative to the total amount of tracer released (units are m^{-2}) measured at individual stations during the cruises listed in Table 1 and shown in Fig. 1. Only a subset of Cruise US2 is shown: US-2A is the latitudinal transect at 96° and US-2B is the latitudinal transect at 93°. The spread in the modeled ensemble mean concentrations, shown as think black lines, is based on the maximum and minimum concentrations at each point of all 12 release experiments.

Fig. 3: (a) Altimetry based (AVISO) time-mean geostrophic current speed averaged from 1993 to 2011. Regions around Antarctica where the AVISO data were missing sometime during the averaging period are left white. (b) Modeled time mean current speed averaged over model integration years 6, 7 and 8. White regions around Antarctica indicate maximum sea ice extent over the 3 year period. The two faint dashed lines are the locations of WOCE sections P18, P19, and A21 shown in Fig. 14.

Fig. 4: (a) AVISO geostrophic eddy current speeds ($EKE^{1/2}$) and (b) modeled eddy current speeds

. The EKE is defined as the temporal fluctuation about the averages shown in Fig. 3.

Fig. 5: Comparison of simulated vertical structure of current speed ($KE^{1/2}$) (black lines) against FDRAKE mooring data from the late 1970's (red lines). The location of each FDRAKE mooring is plotted in the inset. The average length of the mooring data is 320 days. The black line with the largest EKE in the model is from the northernmost mooring location.

Fig. 6: (a) Modeled average ($\mu = N^{-1} \sum c_i$) and (b) standard deviation ($s_N = \sqrt{(N-1)^{-1} \sum (c_i - \mu)^2}$) of the column integrated tracer concentration at the US2 cruise track locations versus time. The tracer concentrations are normalized by the total amount of tracer released, hence the units are m^{-2}. The red 'x' shows the observed tracer concentration and standard deviation from the DIMES US2 cruise, with the red line indicating a 95% confidence interval using bootstrapping. Gray shading indicates a the minimum and maximum values from the 12 tracer releases from the ensemble. (b) and (c) show the same means and standard deviations, but at the times of the cruises listed in Table 1 for the 4 DIMES cruises. he UK2 and UK2.5 cruises have been split into individual transects from west to east (K2A, K2B, K2C and K2.5A and K2.5B respectively. Notice that we used a logarithmic scale in these two panels, because the concentrations drop substantially in the subsequent cruises which were done two to three years after injection.

Fig. 7: Comparison of the average rate of dispersion using: the full model ensemble average tracer (black line), the ensemble average tracer subsampled on the US2 cruise stations (red line with gray shading indicating the minima and maxima from the 12 release experiments), and the observed DIMES tracer during US2 (red 'x'). A 95% confidence interval on the DIMES tracer is estimated using bootstrapping. The blue circle and the blue error bar indicates the extrapolated estimate of the average rate of dispersion over the first year of the DIMES tracer using Eqs. 7 and 8.

Fig. 8: (a) Dispersion σ_y^2 of the ensemble mean tracer in the simulation versus time (blue line). The red line marks the average dispersion in the first year after release, with slope $\sigma_y^2(t)/2t$ where $t = 365$, and the black line marks a least-squares fit to the dispersion from $t = 100$ to $t = 500$. (b) The slopes of the red and black lines in (a) are plotted in (b) as solid red and black lines. The slopes each of each of the 12 tracer release experiments in the ensemble are plotted as red and black x's.

Fig. 9: Dispersion σ_y^2 from model tracers released at four different depths at depths near 500 m, 1 km, 1.5 km, and 2 km (blue lines). The red lines are the average dispersion over the first year and the black lines are the least-squares fit dispersion between day 100 and day 500 as in Fig. 8.

Fig. 10: (a) Estimates of the vertical structure of the isopycnal eddy diffusivity upstream of 75°W at various depths. The eddy diffusivity is estimated as the least-squares fit dispersion between day 100 and day 500 (see Fig. FigDISP:fig). The estimates from the ensemble average tracer released at 1500m is indicated as a black 'x' with the error bar showing the minimum and maximum values from the 12 release experiments. (b) Model estimate of the mean flow, $U(z)$, eddy phase speed, c, and $EKE^{1/2}$, all averaged from 61°S to 56°S and 110°W to 80°W.

Fig. 11: Streamline coordinate system. The s coordinate is along streamlines, the n coordinate in normal to it. The area of the patch A in streamline coordinate is indicated.

Fig. 12: Three model based estimates (left to right) of eddy diffusivity at 1500m in latitude coordinates (top) and streamline coordinates (bottom). The eddy diffusivity is determined as the growth rate of the second moment of the tracer concentration. The three estimates of the second moment in latitude coordinates are: the second moment averaged over the whole area spun by the tracer $\sigma_y^2 =< y^2 c > / < c >$ (left), meridional binning followed by second moment $\sigma_y^2 = \sum y^2 \int c\ dx / \sum \int c\ dx$ (middle), and meridional binning followed by a least-squares fit to a Gaussian using gradient descent (right). The thick black line are estimated based on the ensemble average tracer $\overline{c}$, while the grey the gray lines are estimates based on the individual 12 tracer release experiments..

Fig. 13: Three estimates (left to right) of diffusivity at 1500m in the model using tracer subsampled on the US2 cruise track locations, in latitude coordinates (top) and streamline coordinates (bottom). The eddy diffusivity is determined as the growth rate of the second moment of the tracer concentration. The three estimates of the second moment (in latitude coordinates) are: the second moment $\sigma_y^2 = \sum_i y_i^2 \overline{c}_i / \sum_i \overline{c}_i$ (left), meridionally binned second moment $\sigma_y^2 = \sum_j \left(y_j^2 \sum_i \overline{c}_i \right) / \sum_i \left(\sum_i \overline{c}_i \right)$ where j is a sum over bins and i is a sum over points within each bin (middle), a least-squares fit to a Gussian after binning meridionally.

Fig. 14: Comparison of WOCE (left) neutral density from Section P18 (top), P19 (middle), and A21 (bottom) with the Drake Patch model (right) at 103°W (top), 88°W (middle), and near (68°W,61°S) following A21 (bottom). The WOCE CTD profiles were collected in Early February 2008 (P18), January and March 1993 (P19) and late January 1990 (A21), and were plotted as a section using Delaunay triangulation with cubic interpolation. The modeled sections are snapshots on January 19 of the 6th year of integration for P18, the southern part of P19 and A21, and Feburary 18 for northern part of P19.

Fig. 15: Time evolution of the variance of the tracer spread in density space for a tracer that was injected with a Gaussian concentration in the vertical, advected by advection schemes of Prather (1986) and Daru and Tenaud (2004). The squared half-width $\sigma_\rho(t)^2$ (indicated as continuous lines) is for a Gaussian fitted to the vertical profile of the tracer after integration along neutral density surfaces. A diapycnal eddy diffusivity is estimated as half the growth rate of $\sigma_\rho(t)^2$ (dashed lines). Converting into z-coordinates both schemes imply diapycnal mixing $K^z < 10^{-5}$ m^{2}s^{-1}.